Survey of the Heritability and Sparse Architecture of Gene Expression Traits Across Human Tissues

Short title: Heritability and Sparse Architecture of Gene Expression

Heather E. Wheeler[1,2,*], Kaanan P. Shah[3], Jonathon Brenner[2], Tzintzuni Garcia[4], Keston Aquino-Michaels[3], GTEx Consortium, Nancy J. Cox[5], Dan L. Nicolae[3], Hae Kyung Im[3,*]

1 Department of Biology, Loyola University Chicago, Chicago, IL, USA

2 Department of Computer Science, Loyola University Chicago, Chicago, IL, USA

3 Section of Genetic Medicine, Department of Medicine, University of Chicago, Chicago, IL, USA

4 Center for Research Informatics, University of Chicago, Chicago, IL, USA

5 Division of Genetic Medicine, Vanderbilt University, Nashville, TN, USA

*** hwheeler1@luc.edu, haky@uchicago.edu**

Abstract

For most complex traits, gene regulation is known to play a crucial mechanistic role as demonstrated by the consistent enrichment of expression quantitative trait loci (eQTLs) among trait-associated variants. Thus, understanding the genetic architecture of gene expression traits is key to elucidating the underlying mechanisms of complex traits. However, a systematic survey of the heritability and the distribution of effect sizes across all representative tissues in the human body has not been reported. Here we fill this gap through analyses of the RNA-seq data from a comprehensive set of tissue samples generated by the GTEx Project and the DGN whole blood cohort. We find that local h^2 can be relatively well characterized with 50% of expressed genes showing significant h^2 in DGN and 8-19% in GTEx. However, the current sample sizes ($n < 362$ in GTEx) only allow us to compute distal h^2 for a handful of genes (3% in DGN and <1% in GTEx). Thus, we focus on local regulation. Bayesian Sparse Linear Mixed Model (BSLMM) analysis provide strong evidence that the genetic contribution to expression traits is dominated by a handful of genetic variants rather than by the collective contribution of a large number of variants each of modest size. In other words, that the local architecture of gene expression traits is sparse rather than polygenic across DGN (whole blood) and all 40 GTEx tissues examined. This result is further confirmed by the sparsity of optimal performing gene expression predictors via elastic net modeling. To further explore the tissue context specificity, we decompose the expression traits into cross-tissue and tissue-specific components using a novel Orthogonal Tissue Decomposition approach. Through a series of simulations we show that the cross tissue and tissue specific components are identifiable via OTD. Heritability and sparsity estimates of these derived expression phenotypes show similar characteristics to the original traits. Consistent properties relative to prior GTEx multi-tissue analysis results suggest that these traits reflect the expected biology. Finally, we apply this knowledge to develop prediction models of gene expression traits for all tissues. The prediction models, heritability, and prediction performance R^2 for original and decomposed expression phenotypes are made publicly available (`https://github.com/hakyimlab/PrediXcan`).

Author Summary

Gene regulation is known to contribute to the underlying mechanisms of complex traits. The GTEx project has generated RNA-Seq data on hundreds of individuals across more than 40 tissues providing a comprehensive atlas of gene expression traits. Here, we systematically examined the local versus distant heritability as well as the sparsity versus polygenicity of protein coding gene expression traits in tissues across the entire human body. To determine tissue context specificity, we decomposed the expression levels into cross-tissue and tissue-specific components. Regardless of tissue type, we found that local heritability, but not distal heritability, can be well characterized with current sample sizes. We also find that the distribution of effect sizes is more consistent with a sparse local architecture across all tissues. We also show that the cross-tissue and tissue-specific expression phenotypes constructed with our orthogonal tissue decomposition model recapitulate complex Bayesian multi-tissue analysis results. This knowledge was applied to develop prediction models of gene expression traits for all tissues, which we make publicly available.

Introduction

Regulatory variation plays a key role in the genetics of complex traits [1–3]. Methods that partition the contribution of environment and genetic components are useful tools to understand the biology underlying complex traits. Partitioning heritability into different functional classes (e.g. promoters, coding regions, DNase I hypersensitivity sites) has been successful in quantifying the contribution of different mechanisms that drive the etiology of diseases [3–5].

Most human expression quantitative trait loci (eQTL) studies have focused on how local genetic variation affects gene expression in order to reduce the multiple testing burden that would be required for a global analysis [6, 7]. Furthermore, when both local and distal eQTLs are reported [8–10], effect sizes and replicability are much higher for local eQTLs. While many common diseases are likely polygenic [11–13], it is unclear whether gene expression levels are also polygenic or instead have simpler genetic architectures. It is also unclear how much these expression architectures vary across

genes [6].

BSLMM models complex traits as a mixture of sparse and polygenic contributions. The sparse component consists of a handful of variants of small effect sizes whereas the polygenic component allows for most variants to contribute to the trait albeit with small effect sizes. SOME ADDITIONAL DESCRIPTION OF BSLMM, ASSUMPTIONS, ETC. BSLMM allows us to directly estimate the sparse and polygenic components of a trait.

As a somewhat independent approach to determine the sparsity and polygenicity of gene expression traits traits, we can look at the relative prediction performance of sparse and polygenic models. For example, if the true model of a trait is polygenic, it is natural to expect that polygenic models will predict better (higher predicted vs. observed R^2) than sparse ones. We assessed the ability of various models, with different underlying assumptions, to predict gene expression in order to both understand the underlying genetic architecture of gene expression ~~and to further optimize predictors for our gene-level association method, PrediXcan~~ [14]. For gene expression prediction, we have shown that sparse models such as LASSO (Least Absolute Shrinkage and Selection Operator) perform better than a polygenic score model and that a model that uses the top eQTL variant outperformed the polygenic score but did not do as well as LASSO or elastic net (mixing parameter $\alpha = 0.5$) [14]. These results suggest that for many genes, the genetic architecture is sparse, but not regulated by a single SNP consistent with previous work describing the allelic heterogeneity of gene expression [15–17].

Thus, gene expression traits with sparse architecture should be better predicted with models such as LASSO, which prefers solutions with fewer parameters, each of large effect [18]. Conversely, highly polygenic traits should be better predicted with ridge regression or similarly polygenic models that prefer solutions with many parameters, each of small effect [19–21]. Elastic net [22] is a good multi-purpose model that encompasses both LASSO and ridge regression at its extremes and has been shown to predict well across many complex traits with diverse genetic architectures [23]. TO DELETE: ~~To obtain a more thorough understanding of gene expression architecture, we used the hybrid approaches of the elastic net and BSLMM (Bayesian Sparse Linear Mixed Model)~~ [24] ~~to quantify sparse and polygenic effects~~.

Most previous human eQTL studies were performed in whole blood or

lymphoblastoid cell lines due to ease of access or culturabilty [8, 25, 26]. Although studies with a few other tissues have been published, comprehensive coverage of human tissues was not available until the launching of the Genotype-Tissue Expression (GTEx) Project. GTEx aims to examine the genetics of gene expression more comprehensively and has recently published a pilot analysis of eQTL data from 1641 samples across 43 tissues from 175 individuals [27]. Here we use a much larger set of 8555 samples across 53 tissues corresponding to 544 individuals. One of the findings of this comprehensive analysis was that a large portion of the local regulation of expression traits is shared across multiple tissues. Corroborating this finding, our prediction model built in DGN whole blood showed robust prediction [14] across the nine tissues with the largest sample size from the GTEx Pilot Project [27].

This shared regulation implies that there is much to be learned from large sample studies of easily accessible tissues. Yet, a portion of gene regulation seems to be tissue dependent [27]. To further investigate the genetic architecture that is common across tissues or specific to each tissue, ~~In order to harness this cross-tissue effect for prediction and to better understand the genetic architecture of tissue-specific and cross-tissue gene regulation~~ we use a mixed effects model called orthogonal tissue decomposition (OTD) and sought to decouple the cross-tissue and tissue-specific mechanisms in the rich GTEx dataset. We show that the cross-tissue and tissue-specific expression phenotypes constructed with our orthogonal tissue decomposition model reflect the expected biology. ~~We also show that the local common variant architecture of gene expression is sparse, which allows accurate prediction at current sample sizes.~~

Results

Significant local heritability of gene expression in all tissues

We estimated the local and distal heritability of gene expression levels in 40 tissues from the GTEx consortium and whole blood from the Depression Genes and Networks (DGN) cohort. The sample size in GTEx varied from 72 to 361 depending on the tissue, while 922 samples were available in DGN [26]. We used linear mixed models (see Methods) and calculated variances using restricted maximum likelihood (REML) as

implemented in GCTA [28].

For the local heritability component, we used common (minor allele frequency > 0.05) variants within 1Mb of the transcription start and end of each protein coding gene, whereas for the distal component, we used common variants outside of the chromosome where the gene was located. Different approaches to pick the set of distal variants were explored, but results were robust to different selections (see Methods).

Table 1 summarizes the local heritability estimate results across all tissues. In order to obtain an unbiased estimates of mean h^2 across genes, we do not constrain the model to only output h^2 estimates between 0 and 1. Instead, as done previously [10, 29], we allow the h^2 estimates to be negative when fitting the model and thus refer to it as the unconstrained REML. This approach reduces the standard error of the estimated mean of heritability, especially important for the distal component. Even though each individual gene's distal heritability is noisy (Fig. 1), averaging across all genes reduces the error for the mean estimate substantially. For the DGN dataset, we were able to estimate the mean distal h^2, which was 0.034 (SE = 0.0024). However for the GTEx samples, the sample size was too small and the REML algorithm became unstable (did not converge) when allowing for negative values. This numeric instability would cause only a small number of genes (< 10%) with large positive (and noisy) heritability values to converge biasing the mean value. For this reason we do not show mean distal heritability estimates for GTEx tissues.

Gene expression local heritability estimates were consistent between whole blood tissue from the DGN and GTEx cohorts (Spearman's $\rho = 0.28$ [95% confidence interval (CI): 0.27-0.29]). DGN estimates made here were also consistent with those made in independent blood cohorts from previous studies. Comparing DGN to Price et al. [29] and Wright et al. [10], $\rho = 0.31$ [0.30-0.32] and 0.083 [0.070-0.095], respectively. Spearman's ρ between Price et al. [29] and Wright et al. [10] gene expression heritability estimates was 0.12 [0.11-0.14].

The left column of Fig. 1 shows the estimated local and distal h^2 from DGN. Even though many genes show relatively large point estimates of distal h^2, only those colored in blue are significantly different from zero (Fig. 1, uncorrected $P < 0.05$). The local component of h^2 is relatively well estimated in DGN with 50% of genes (6399 out of 12719) showing $P < 0.05$ (FDR = 0.099). In contrast, the distal heritability is significant

for only 7.3% (931 out of 12719) of the genes ($P < 0.05$). This is not much larger than the expected number at this significance level (5%) and the genes with $P < 0.05$ and negative h^2 in Fig. 1 are obvious false positives, within the type 1 error rate.

It has been shown that local-eQTLs are more likely to be distal-eQTLs of target genes [30]. Thus, we tested whether restricting the distal h^2 estimates to known eQTLs on non-gene chromosomes could improve distal h^2 precision by prioritizing functional variants. We defined the known eQTLs by using the Framingham mRNA cohort of over 5000 individuals [31] (see Methods), which is independent from the DGN and GTEx cohorts. While using known eQTLs to define distal h^2 decreased the 95% CI mean across genes from [-0.45-0.50] to [-0.26-0.29], the number of significant genes did not change dramatically (Fig. 1). Also, using the subset of known eQTLs reduced the mean distal h^2 from 0.027 to 0.015. Therefore, while we gain some power to detect significant distal h^2 by using eQTL priors as indicated by the standard error reduction, a good portion of the distal regulation is lost when using only the smaller subset of known eQTLs. When we used known eQTLs to estimate distal h^2 in the GTEx cohort, less than 1% of genes had a $P < 0.05$ (S1 Fig). The two different methods to define distal h^2 did not affect the local h^2 estimates (Spearman's $\rho = 0.86$), demonstrating the robustness of local h^2 component in the linear mixed model. Given the limited sample size we will focus on local regulation for the remainder of the paper.

To determine if the local estimates were affected by linkage disequilibrium (LD), we also estimated the local heritability of gene expression in the DGN cohort using LDAK, a software for computing LD-adjusted kinships [32]. While the estimates were slightly higher using GCTA (mean = 0.143) compared to LDAK (mean = 0.118), the Pearson correlation between h^2 estimates from GCTA and LDAK was high (R=0.96), indicating that the local component of heritability using either method is about the same (S2 Fig).

Table 1. Estimates of unconstrained local h^2 across genes within tissues.

tissue	n	mean h^2 (SE)	% q-val<0.1	num q-val<0.1	num expressed
DGN Whole Blood	922	0.143 (0.0039)	50.4	6407	12719
Cross-tissue	450	0.062 (0.017)	31.9	5399	16951
Adipose - Subcutaneous	298	0.038 (0.028)	9.2	1312	14205
Adrenal Gland	126	0.043 (0.018)	3.2	453	14150
Artery - Aorta	198	0.042 (0.024)	7.6	1046	13844
Artery - Coronary	119	0.037 (0.048)	2.1	297	14127
Artery - Tibial	285	0.042 (0.02)	10.1	1364	13504
Brain - Anterior cingulate cortex (BA24)	72	0.028 (0.036)	0.9	124	14515
Brain - Caudate (basal ganglia)	100	0.037 (0.047)	1.8	265	14632
Brain - Cerebellar Hemisphere	89	0.049 (0.068)	3.3	470	14295
Brain - Cerebellum	103	0.050 (0.06)	4.3	625	14491
Brain - Cortex	96	0.045 (0.057)	2.2	317	14689
Brain - Frontal Cortex (BA9)	92	0.038 (0.077)	1.6	240	14554
Brain - Hippocampus	81	0.037 (0.05)	0.6	94	14513
Brain - Hypothalamus	81	0.017 (0.043)	0.7	104	14759
Brain - Nucleus accumbens (basal ganglia)	93	0.029 (0.04)	1.3	195	14601
Brain - Putamen (basal ganglia)	82	0.032 (0.064)	0.9	135	14404
Breast - Mammary Tissue	183	0.029 (0.037)	3.4	493	14700
Cells - EBV-transformed lymphocytes	115	0.058 (0.1)	3.6	451	12454
Cells - Transformed fibroblasts	272	0.051 (0.031)	11.8	1510	12756
Colon - Sigmoid	124	0.033 (0.019)	3.0	425	14321
Colon - Transverse	170	0.036 (0.058)	4.3	625	14676
Esophagus - Gastroesophageal Junction	127	0.032 (0.039)	2.3	319	14125
Esophagus - Mucosa	242	0.042 (0.03)	9.2	1306	14239
Esophagus - Muscularis	219	0.039 (0.015)	8.2	1148	14047
Heart - Atrial Appendage	159	0.042 (0.03)	4.2	579	13892
Heart - Left Ventricle	190	0.034 (0.034)	5.5	733	13321
Liver	98	0.033 (0.062)	1.4	195	13553
Lung	279	0.032 (0.034)	7.2	1070	14775
Muscle - Skeletal	361	0.033 (0.03)	9.5	1221	12833
Nerve - Tibial	256	0.052 (0.087)	11.9	1725	14510
Ovary	85	0.037 (0.094)	0.9	123	14094
Pancreas	150	0.047 (0.024)	5.1	716	13941
Pituitary	87	0.038 (0.055)	1.7	252	15183
Skin - Not Sun Exposed (Suprapubic)	196	0.041 (0.034)	5.1	754	14642
Skin - Sun Exposed (Lower leg)	303	0.039 (0.016)	9.8	1439	14625
Small Intestine - Terminal Ileum	77	0.036 (0.053)	0.6	94	14860
Spleen	89	0.059 (0.061)	2.2	319	14449
Stomach	171	0.032 (0.025)	3.3	484	14531
Testis	157	0.054 (0.044)	7.8	1325	16936
Thyroid	279	0.044 (0.066)	10.8	1583	14642
Whole Blood	339	0.033 (0.023)	8.6	1042	12160

Except for DGN Whole Blood, all tissues are from the GTEx Project. Cross-tissue uses derived expression levels from our orthogonal tissue decomposition (OTD) of GTEx data. Mean heritability (h^2) and the standard error of the mean (SE) are calculated across genes for each tissue. The percentage (%) and number (num) of genes with significant h^2 estimates ($P < 0.05$) and the number of genes expressed in each tissue are also reported. FDR is the false discovery rate at the $P < 0.05$ threshold.

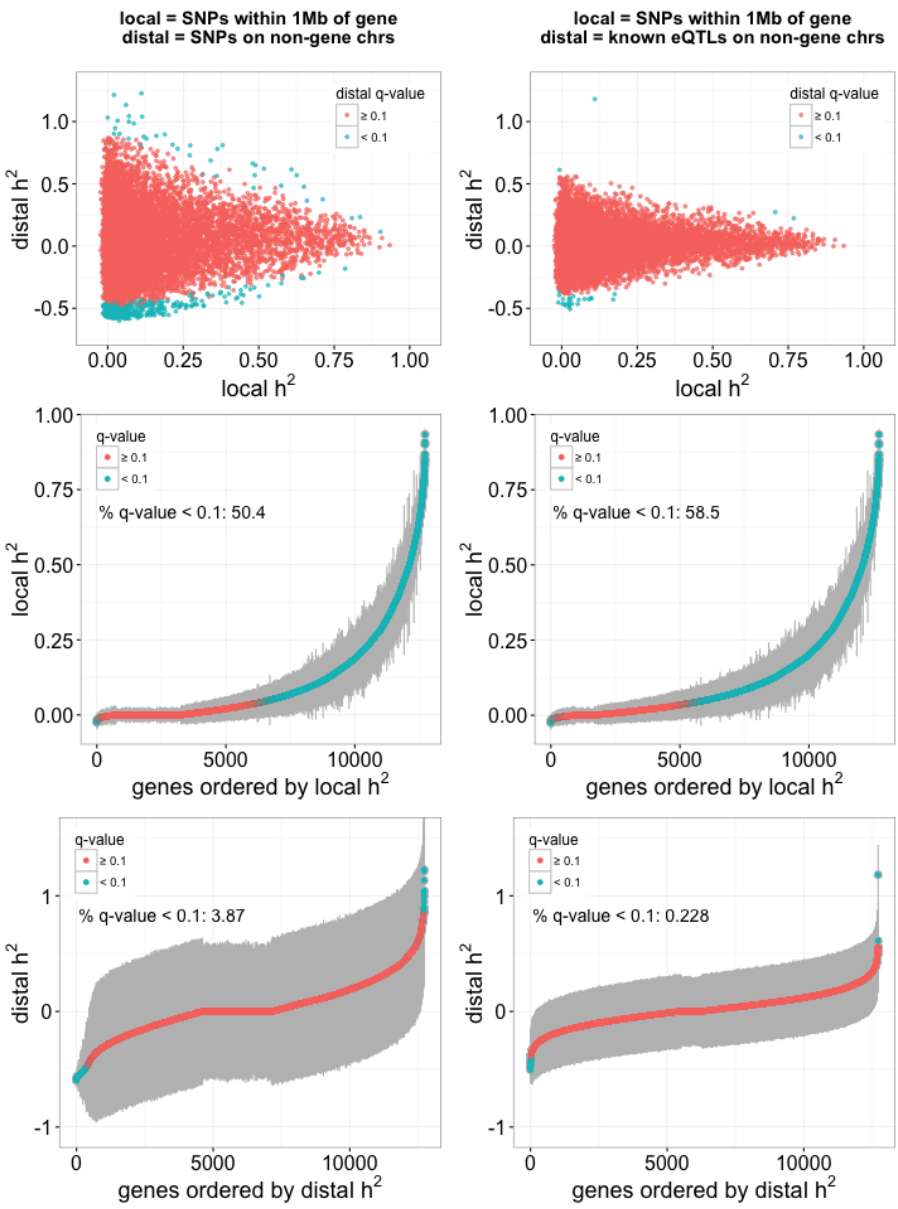

Figure 1. DGN whole blood expression local and distal heritability (h^2). This figure shows the local and distal heritability of gene expression levels in whole blood from the DGN RNA-seq dataset. In order to obtain an unbiased estimates of mean h^2, we allow the values to be negative when fitting the REML (unconstrained). Notice that only a few genes have distal heritability that is significantly different from 0 ($P < 0.05$). Local was defined as 1Mb from each gene. For the left side panel, distal heritability was computed using all SNPs outside of the gene's chromosome. On the the right side, distal heritability was computing using SNPs that were cis-eQTLs in the Framingham study. (**Top**) Distal h^2 compared to local h^2 per gene in each model. (**Middle**) Local and (**Bottom**) distal gene expression h^2 estimates ordered by increasing h^2. As a measure of uncertainty, we have added two times the standard errors of each h^2 estimate in gray segments. Genes with significant h^2 ($P < 0.05$) are shown in blue. To be conservative, we set $h^2 = 0$ when GCTA did not converge. Genes in blue with negative h^2 are false positives, within the type 1 error (5%).

Prediction models with a sparse component outperform polygenic models

Next, we sought to determine whether the local common genetic contribution to gene expression is polygenic or sparse. In other words, whether many variants with small effects or a small number of large effects were contributing to expression trait variability. For this, we first looked at the prediction performance of a range of models with different degrees of polygenicity, such as the elastic net model with mixing parameter values ranging from 0 (fully polygenic, ridge regression) to 1 (sparse, LASSO).

More specifically, we performed 10-fold cross-validation using the elastic net [22] to test the predictive performance of local SNPs for gene expression across a range of mixing parameters (α). Given common folds and seeds, the mixing parameter that yields the largest cross-validation R^2 informs the degree of sparsity of each gene expression trait. That is, at one extreme, if the optimal $\alpha = 0$ (equivalent to ridge regression), the gene expression trait is highly polygenic, whereas if the optimal $\alpha = 1$ (equivalent to LASSO), the trait is highly sparse. We found that for most gene expression traits, the cross-validated R^2 was smaller for $\alpha = 0$ and $\alpha = 0.05$, but nearly identical for $\alpha = 0.5$ through $\alpha = 1$ in the DGN cohort (Fig. 2). An $\alpha = 0.05$ was also clearly suboptimal for gene expression prediction in the GTEx tissues, while models with $\alpha = 0.5$ or 1 had similar predictive power (S3 Fig). This suggests that for most genes, the effect of local common genetic variation on gene expression is sparse rather than polygenic.

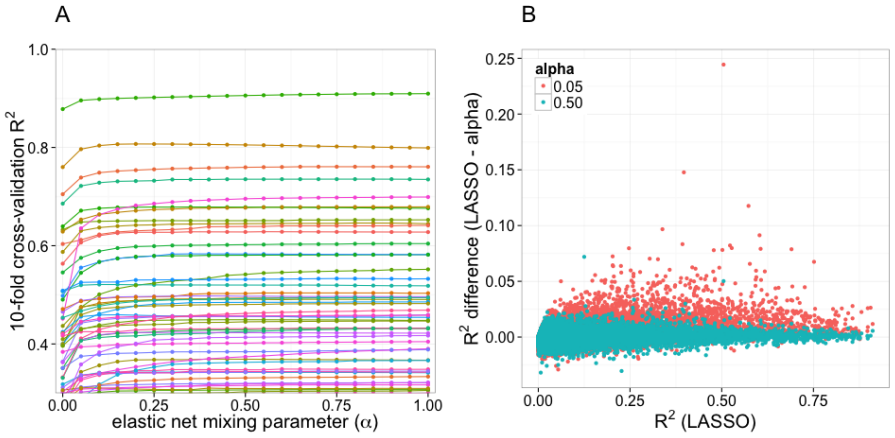

Figure 2. DGN cross-validated predictive performance across the elastic net. This figure shows the cross validated R^2 between observed and predicted expression levels using elastic net prediction models in DGN whole blood. (**A**) This panel shows the 10-fold cross validated R^2 for 51 genes with $R^2 > 0.3$ from chromosome 22 as a function of the elastic net mixing parameters (α). Smaller mixing parameters correspond to more polygenic models while larger ones correspond to more sparse models. Each line represents a gene. The performance is in general flat for most values of the mixing parameter except very close to zero where it shows a pronounced dip. Thus polygenic models perform more poorly than sparse models. (**B**) This panel shows the difference between the cross validated R^2 of the LASSO model and the elastic net model mixing parameters 0.05 and 0.5 for autosomal protein coding genes. Elastic net with $\alpha = 0.5$ values hover around zero, meaning that it has similar predictive performance to LASSO. The R^2 difference of the more polygenic model (elastic net with $\alpha = 0.05$) is mostly above the 0 line, indicating that this model performs worse than the LASSO model.

Sparse local architecture revealed by direct estimation using BSLMM

To further confirm the local sparsity of gene expression traits, we turned to the BSLMM [24] approach, which models the genetic contribution as the sum of a sparse and a highly polygenic component. The parameter PGE in this model represents the proportion of genetic variance explained by sparse effects. Another parameter, the total variance explained (PVE) by additive genetic variants, is a more flexible Bayesian equivalent of the heritability we have estimated using a linear mixed model (LMM) as implemented in GCTA.

For genes with low heritability, our power to discern between sparse and polygenic architecture is limited. In contrast, for highly heritable genes, the credible sets are tighter and we are able to determine that the sparse component is large. For example,

all genes with heritability > 0.50 had the proportion of sparse component that was > 0.82 half of which had PGE close to 1 (Fig. 3A). Half of the genes with heritability above 0.1 had PGE > 0.949. Fittingly, for most (96.3%) of the genes with heritability > 0.10, the number of SNPs included in the model was below 10.

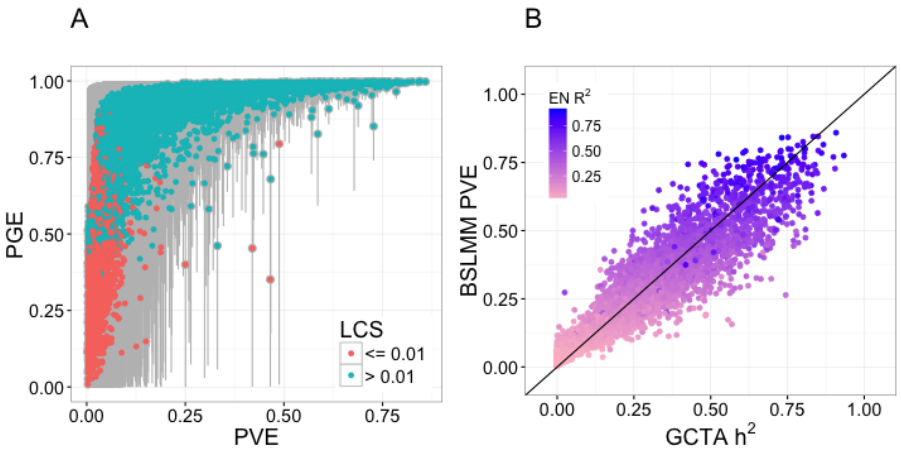

Figure 3. Sparsity estimates using Bayesian Sparse Linear Mixed Models in DGN whole blood. (**A**) This panel shows a measure of sparsity of the gene expression traits represented by the PGE parameter from the BSLMM approach. PGE is the proportion of the sparse component of the total variance explained by genetic variants, PVE (the BSLMM equivalent of h^2). The median of the posterior samples of BSLMM output is used as estimates of these parameters. Genes with a lower credible set (LCS) > 0.01 are shown in blue and the rest in red. The 95% credible set of each estimate is shown in gray. For highly heritable genes the sparse component is close to 1, thus for high heritability genes the local architecture is sparse. For lower heritability genes, there is not enough evidence to determine sparsity or polygenicity. (**B**) This panel shows the heritability estimate from BSLMM (PVE) vs the estimates from GCTA, which are found to be similar (R=0.96). Here, the estimates are constrained to be between 0 and 1 in both models. Each point is colored according to that gene's elastic net $\alpha = 1$ cross-validated prediction correlation squared (EN R^2). Note genes with high heritability have high prediction R^2.

BSLMM outperforms LMM in estimating h^2 for small samples

In DGN, there is a strong correlation between BSLMM-estimated PVE and GCTA-estimated h^2 (Fig. 3B, R=0.96). In contrast, when we applied BSLMM to the GTEx data, we found that many genes had measurably larger BSLMM-estimated PVE than LMM-estimated h^2 (Fig. 4). This is further confirmation of the local sparse architecture of gene expression traits: the underlying assumption in the LMM approach to estimate heritability is that the genetic effect sizes are normally distributed, i.e. most variants have small effect sizes. LMM is quite robust to departure from this assumption,

but only when the sample size is rather large (S4 Fig). For the relatively small sample sizes in GTEx ($n \leq 361$), we found that directly modeling the sparse component with BSLMM (polygenic + sparse components) outperforms LMM (single polygenic component) for estimating h^2. Here, unlike in previous sections (see Fig. 1 and Table 1), both the BSLMM and LMM model estimates are constrained to be between 0 and 1. The genes with high BSLMM PVE and near zero LMM h^2 have high cross-validated R^2 from the elastic net $\alpha = 1$ results, providing strong evidence that heritability is not zero and that the underlying genetic architecture is sparse for these genes. (Fig. 4).

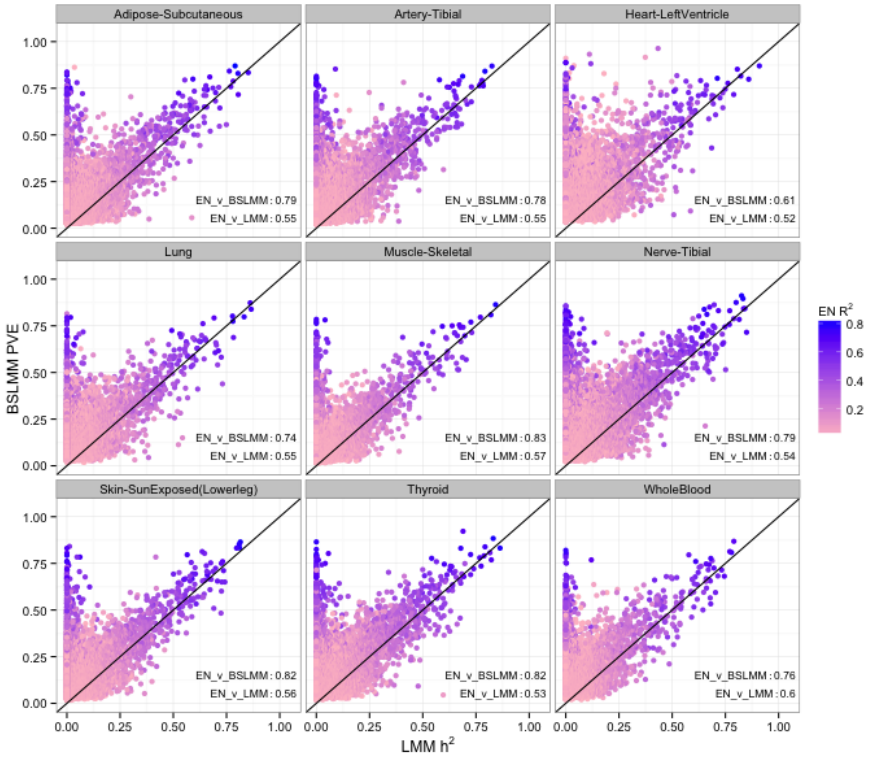

Figure 4. BSLMM vs LMM estimates of heritability in GTEx. This figure shows the comparison between estimates of heritability using BSLMM vs. LMM (GCTA) for GTEx data. Here, in both models the estimates are constrained to be between 0 and 1. For most genes BSLMM estimates are larger than LMM estimates reflecting the fact that BSLMM yields higher estimates of heritability because of its ability to account for the sparse component. Each point is colored according to that gene's elastic net $\alpha = 1$ cross-validated prediction correlation squared (EN R^2). Comparing EN R^2 to the heritability estimates, the Pearson correlations with BSLMM (EN_v_BSLMM) are higher than those with LMM (EN_v_LMM) for all tissues, consistent with a sparse genetic architecture of gene expression.

Orthogonal decomposition of cross-tissue and tissue-specific expression traits

Since a substantial portion of local regulation was shown to be common across multiple tissues [27], we sought to decompose the expression levels into a component that is common across all tissues and tissue-specific components. Figure 5 shows a diagram describing the decomposition. For this we use a linear mixed effects model with a person-level random effect. See details in Methods. We use the posterior mean of this random effect as an estimate of the cross-tissue component. We consider the residual component of this model as the tissue-specific component. We call this approach orthogonal tissue decomposition (OTD) because the cross-tissue and tissue-specific components are assumed to be independent in the model.

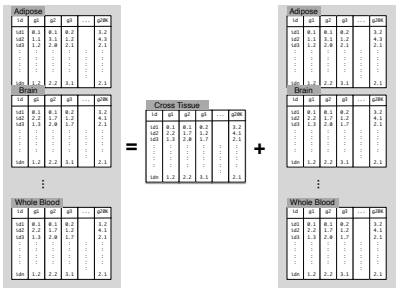

Figure 5. Orthogonal Tissue Decomposition of gene expression traits.

First we demonstrate that this approach is able to identify the cross tissue and tissue specific components via simulations. We generate simulated traits so that the true cross tissue and tissue specific components are known. To preserve the correlation structure between genes and tissues, we take the estimated cross tissue and tissue specific components as the true values. Then simulate expression traits as the sum of the cross tissue and tissue specific components and an error term (expression trait = cross tissue + tissue specific + noise). We simulate expression traits using different magnitude of the noise level and apply our OTD approach. In Figure S5 we show for one simulated example the correlation between true and OTD-estimated components for one gene, SLTM (A) and the distribution of the correlation between true and OTD-estimates for all genes. The median Pearson correlation between true and OTD-estimted cross-tissue components was 0.54 [95% CI: 0.33-0.77] and for tissue-specific component was 0.75 [0.46-0.88], demonstrating the robustness of our model (S5 Fig).

For the OTD derived cross-tissue and 40 tissue-specific expression phenotypes, we computed the local heritability and generated prediction models. The decomposition is applied at the expression trait level so that the downstream genetic regulation analysis is performed separately for each derived trait, cross-tissue and tissue-specific expression, which greatly reduces computational burden.

Cross-tissue expression phenotype is less noisy and shows higher predictive performance

Our estimates of h^2 for cross-tissue expression traits are larger than the corresponding estimates for each whole tissue expression traits (S6 Fig). This is due to the fact that our OTD approach increases the ratio of genetically regulated component to noise by averaging across multiple tissues. In addition to the increased h^2 we observe reduction in standard errors of the estimated h^2. This is due, in part, to the larger effective sample size for cross-tissue phenotypes. There were 450 samples for which cross-tissue traits were available whereas the maximum sample size for whole tissue phenotypes was 362. As consequence of this increased h^2 and decreased standard errors, the percentage of cross h^2 estimates with $P < 0.05$ was 35.4% whereas for whole tissue expression traits they ranged from 8.5-19.0% (Table 1). Similarly, cross-tissue BSLMM PVE estimates had lower error than whole tissue PVE (S7 Fig, S8 Fig).

As for the tissue-specific components, the cross-tissue heritability estimates were also larger and the standard errors were smaller reflecting the fact that a substantial portion of regulation is common across tissues (S9 Fig). The percentage of GCTA h^2 estimates with $P < 0.05$ was much larger for cross-tissue expression (35.4%) than the tissue-specific expressions (7.6-17.7%, S1 Table). Similarly, the percentage of BSLMM PVE estimates with a lower credible set greater than 0.01 was 49% for cross-tissue expression, but ranged from 24-27% for tissue-specific expression (S8 Fig).

Cross-tissue predictive performance exceeded that of both tissue-specific and whole tissue expression as indicated by higher cross-validated R^2 (S2 Fig, S9 Fig). Like whole tissue expression, cross-tissue and tissue-specific expression showed higher predictive performance when using more sparse models. In other words elastic-net models with $\alpha \geq 0.5$ predicted better than the ones with $\alpha = 0.05$ (S10 Fig).

Cross-tissue expression phenotype recapitulates published multi-tissue eQTL results

To verify that the cross-tissue phenotype has the properties we expect, we compared our OTD results to those from a joint multi-tissue eQTL analysis [33], which was previously performed on a subset of the GTEx data [27] covering 9 tissues. In particular, we used the posterior probability of a gene being actively regulated (PPA) in a tissue. These analysis results are available on the GTEx portal.

First, we reasoned that genes with high cross-tissue h^2 would be actively regulated in most tissues so that the PPA of a gene would be roughly uniform across tissues. By contrast, a gene with tissue-specific regulation would have concentrated posterior probability in one or a few tissues. Thus we decided to define a measure of uniformity of the posterior probability vector across the 9 tissues using the concept of entropy. More specifically, for each gene we normalized the vector of posterior probabilities so that the sum equaled 1. Then we applied the usual entropy definition (negative of the sum of the log of the posterior probabilities weighted by the same probabilities, see Methods). In other words, we defined a uniformity statistic that combines the nine posterior probabilities into one value such that higher values mean the gene regulation is more uniform across all nine tissues, rather than in just a small subset of the nine.

Thus we expected that genes with high cross-tissue heritability, i.e. large cross-tissue regulation would show high probability of being active in multiple tissues, thus high uniformity measure. Reassuringly, this is exactly what we find. Genes with high cross-tissue heritability concentrate on the higher end of the uniformity measure (Fig. 6, S11 Fig).

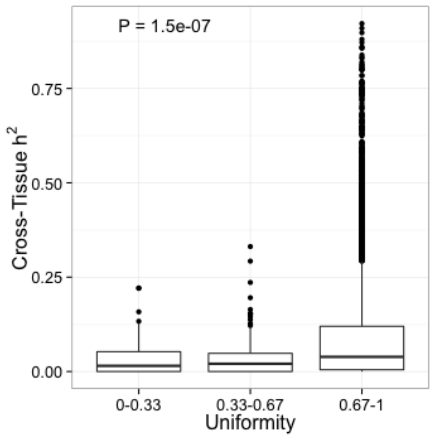

Figure 6. Measure of uniformity of the posterior probability of active regulation vs. cross-tissue heritability. This figure shows the distribution of heritability of the cross-tissue component vs. a measure of uniformity of genetic regulation across tissues. The measure of uniformity was computed using the posterior probability of a gene being actively regulated in a tissue, PPA, from the Flutre et al. [33] multi-tissue eQTL analysis. Genes with PPA concentrated in one tissue were assigned small values of the uniformity measure whereas genes with PPA uniformly distributed across tissues were assigned high value of uniformity measure. See Methods for the entropy-based definition of uniformity. The Kruskal-Wallis rank sum test revealed a significant difference in the cross-tissue h^2 of uniformity groups ($\chi^2 = 31.4$, $P = 1.5\ 10^{-7}$).

For the original whole tissue, we expected the whole tissue expression heritability to correlate with the posterior probability of a gene being actively regulated in a tissue. This is confirmed in Figure 7A where PPA in each tissue is correlated with the BSLMM PVE of the expression in that tissue. In the off diagonal elements we observe high correlation between tissues, which was expected given that large portion of the regulation has been shown to be common across tissues. Whole blood has the lowest correlation consistent with whole blood clustering aways from other tissues [27]. In contrast, panel B of Figure 7 shows that the tissue-specific expression PVE correlates well with matching tissue PPA but the off diagonal correlations are substantially reduced consistent with these phenotypes representing tissue-specific components. Again whole blood shows a negative correlation which could be indicative of some over correction of the cross-tissue component. Overall these results indicate that the cross-tissue and tissue-specific phenotypes have properties that are consistent with the intended decomposition.

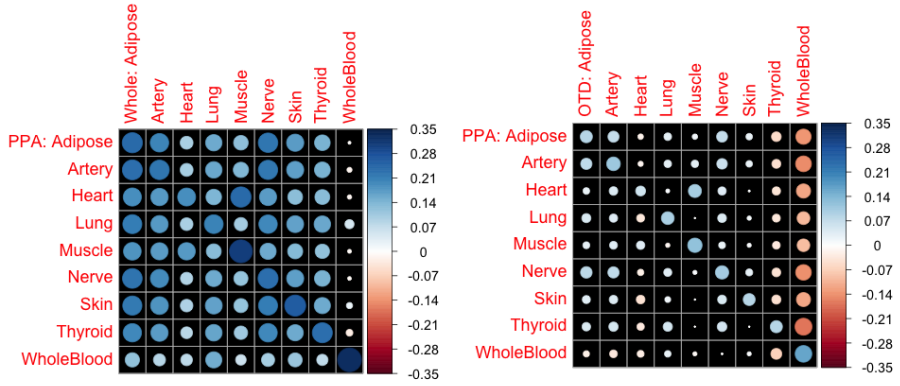

Figure 7. Comparison of heritability of whole tissue or tissue-specific components vs. PPA. Panel (**A**) of this figure shows the Pearson correlation (R) between the BSLMM PVE of the original (we are calling whole here) tissue expression levels vs. the probability of the tissue being actively regulated in a given tissue (PPA). Matching tissues show, in general, the largest correlation values but most of the off diagonal correlations are also relatively high consistent with the shared regulation across tissues. Panel (**B**) shows the Pearson correlation between the PVE of the tissue-specific component of expression via orthogonal tissue decomposition (OTD) vs. PPA. Correlations are in general lower but matching tissues show the largest correlation. Off diagonal correlations are reduced substantially consistent with properties that are specific to each tissue. Area of each circle is proportional to the absolute value of R.

Discussion

Motivated by the key role that regulatory variation plays in the genetic control of complex traits [1–3], we performed a survey of the heritability and patterns of effect sizes of gene expression traits across a comprehensive set of human tissues. We quantified the local and distal heritability of gene expression in DGN and 40 different tissues from the GTEx consortium. For the DGN dataset, we estimate the relative proportion of mean local and distal genetic contribution to gene expression traits. For GTEx samples it was not possible to estimate the mean distal heritability because of the limited sample size. As sample sizes grow to thousands of individuals, we expect to be able to estimate these values.

In DGN (whole blood), the mean local h^2 was 14.3% and the mean distal h^2 was 3.4% such that the local variation contribution is estimated as 14.3/(3.4+14.3) = 81%. This is much higher than the 37% reported by Price et al. [29] based on blood expression data from a cohort of Icelandic individuals using identity by descent, which

captures both common and any rare variation. In addition, our potentially underestimation of the distal component could be due to over-correction of confounders used in the preprocessing of the expression trait data we used. Indeed, PEER [34], SVA [35], and other types of hidden confounder corrections have been shown to increase local eQTL replicability, but their consequences on distal regulation is not well understood. As larger sample sizes become available, we will test this hypothesis in GTEx data by computing the distal h^2 without PEER factor correction. We showed that restricting distal variants to known functional variants such as eQTL data from independent studies improves the precision of distal heritability estimates, but also reduces mean distal heritability estimates by half.

Using results implied by the improved predictive performance of sparse models and by directly estimating sparsity using BSLMM (Bayesian Sparse Linear Mixed Model), we show evidence that for highly heritable genes, local common variant regulation is sparse across all the tissues analyzed here. We note that any rare variants not tagged by common variants are not included in our heritability estimates and prediction models. For genes with moderate and low heritability the evidence is not as strong, but results are consistent with a sparse local architecture. Sparse models capture the most variance in gene expression at current sample sizes and have been used successfully in gene expression prediction methods [14, 36–38]. Better methods to correct for hidden confounders that do not dilute distal signals and larger sample sizes will be needed to determine the properties of distal regulation.

Given that a substantial portion of local regulation is shared across tissues, we propose here to decompose the expression traits into cross-tissue and tissue-specific components. This approach, called orthogonal tissue decomposition (OTD), aims to decouple the shared regulation from the tissue-specific regulation. We examined the genetic architecture of these derived traits and find that they follow similar patterns to the original whole tissue expression traits. The cross-tissue component benefits from an effectively larger sample size than any individual tissue trait, which is reflected in more accurate heritability estimates and consistently higher prediction performance. Encouragingly, we find that genes with high cross-tissue heritability tend to be regulated more uniformly across tissues. As for the tissue-specific expression traits, we found that they recapitulate correlation with the vector of probability of tissue-specific

regulation. Many groups have proposed integrating genotype and expression data to understand complex traits [14, 21, 37–40]. Through integration of our OTD expression traits with studies of complex diseases, we expect results from the cross-tissue models to relate to mechanisms that are shared across multiple tissues, whereas results from the tissue-specific models will inform us about the context specific mechanisms.

In this paper, we quantitate the genetic architecture of gene expression and develop predictors across tissues. We show that local heritability can be accurately estimated across tissues, but distal heritability cannot be reliably estimated at current sample sizes. Using two different approaches, the elastic net and BSLMM, we show that for common local gene regulation, the genetic architecture is mostly sparse rather than polygenic. Using new expression phenotypes generated in our OTD model, we show that cross-tissue predictive performance exceeded that of both tissue-specific and whole tissue expression as indicated by higher elastic net cross-validated R^2. Predictors, heritability estimates and cross-validation statistics generated in this study of gene expression architecture are freely available (`https://github.com/hakyimlab/PrediXcan`) for use in future studies of complex trait genetics.

Methods

Genomic and Transcriptomic Data

DGN Dataset. We obtained whole blood RNA-seq and genome-wide genotype data for 922 individuals from the Depression Genes and Networks (DGN) cohort [26], all of European ancestry. For all analyses, we used the HCP (hidden covariates with prior) normalized gene-level expression data used for the *trans*-eQTL analysis in Battle et al. [26] and downloaded from the NIMH repository. The 922 individuals were unrelated (all pairwise $\hat{\pi} < 0.05$) and thus all included in downstream analyses. Imputation of approximately 650K input SNPs (minor allele frequency [MAF] > 0.05, Hardy-Weinberg Equilibrium [$P > 0.05$], non-ambiguous strand [no A/T or C/G SNPs]) was performed on the Michigan Imputation Server (`https://imputationserver.sph.umich.edu/start.html`) [41, 42] with the following parameters: 1000G Phase 1 v3 ShapeIt2 (no singletons) reference panel, SHAPEIT

phasing, and EUR population. Approximately 1.9M non-ambiguous strand SNPs with MAF > 0.05, imputation $R^2 > 0.8$ and, to reduce computational burden, inclusion in HapMap Phase II were retained for subsequent analyses.

GTEx Dataset. We obtained RNA-seq gene expression levels from 8555 tissue samples (53 unique tissue types) from 544 unique subjects in the GTEx Project [27] data release on 2014-06-13. Of the individuals with gene expression data, genome-wide genotypes (imputed with 1000 Genomes) were available for 450 individuals. While all 8555 tissue samples were used in the OTD model (described below) to generate cross-tissue and tissue-specific components of gene expression, we used the 40 tissues with the largest sample sizes ($n > 70$) when quantifying tissue-specific effects (see Table 1). Approximately 2.6M non-ambiguous strand SNPs included in HapMap Phase II were retained for subsequent analyses.

Framingham Expression Dataset. We obtained exon array expression and genotype array data from 5257 individuals from the Framingham Heart Study [31]. The final sample size after quality control was 4286. We used the Affymetrix power tools (APT) suite to perform the preprocessing and normalization steps. First the robust multi-array analysis (RMA) protocol was applied which consists of three steps: background correction, quantile normalization, and summarization [43]. The background correction step uses antigenomic probes that do not match known genome sequences to adjust the baseline for detection, and is applied separately to each array. Next, the normalization step utilizes a 'sketch' quantile normalization technique instead of a memory-intensive full quantile normalization. The benefit is a much lower memory requirement with little accuracy trade-off for large sample sets such as this one. Next, the adjusted probe values were summarized (by the median polish method) into log-transformed expression values such that one value is derived per exon or gene. In addition, an analysis of the detection of probes above the background noise (DABG) was carried out. It provides further diagnostic information which can be used to filter out poorly performing probes and weakly expressed genes. The summarized expression values were then annotated more fully using the annotation databases contained in the huex10stprobeset.db (exon-level annotations) and huex10sttranscriptcluster.db

(gene-level annotations) R packages available from Bioconductor [44, 45]. In both cases gene annotations were provided for each feature.

Plink [46] was used for data wrangling and cleaning steps. The data wrangling steps included updating probe IDs, unifying data to the positive strand, and updating locations to GRCh37. The data cleaning steps included a step to filter for variant and subject missingness and minor alleles, one to filter variants with Hardy-Weinberg exact test, and a step to remove unusual heterozygosity. To make our data compatible with the Haplotype Reference Consortium (HRC) panel (`http://www.well.ox.ac.uk/~wrayner/tools/`), we used the HRC-check-bin tool in order to carry out data wrangling steps required. The data were then split by chromosome and pre-phased with SHAPEIT [47] using the 1000 Genomes phase 3 panel and converted to vcf format. These files were then submitted to the Michigan Imputation Server (`https://imputationserver.sph.umich.edu/start.html`) [41, 42] for imputation with the HRC version 1 panel [48]. We applied Matrix eQTL [49] to the normalized expression and imputed genotype data to generate prior eQTLs for our heritability analysis.

Partitioning local and distal heritability of gene expression

Motivated by the observed differences in regulatory effect sizes of variants located in the vicinity of the genes and distal to the gene, we partitioned the proportion of gene expression variance explained by SNPs in the DGN cohort into two components: local (SNPs within 1Mb of the gene) and distal (eQTLs on non-gene chromosomes) as defined by the GENCODE [50] version 12 gene annotation. We calculated the proportion of the variance (narrow-sense heritability) explained by each component using the following mixed-effects model:

$$Y_g = \sum_{k \in local} w_{k,g}^{\text{local}} X_k + \sum_{k \in distal} w_{k,g}^{\text{distal}} X_k + \epsilon$$

where Y_g represents the expression of gene g, X_k is the allelic dosage for SNP k, local refers to the set of SNPs located within 1Mb of the gene's transcription start and end, distal refers to SNPs in other chromosomes, and ϵ is the error term representing environmental and other unknown factors. We assume that the local and distal

components are independent of each other as well as independent of the error term. We assume random effects for $w_{k,g}^{\text{local}} \sim N(0, \sigma^2_{w,\text{local}})$, $w_{k,g}^{\text{distal}} \sim N(0, \sigma^2_{w,\text{distal}})$, and $\epsilon \sim N(0, \sigma^2_\epsilon I_n)$, where I_n is the identity matrix. We calculated the total variability explained by local and distal components using restricted maximum likelihood (REML) as implemented in the GCTA software [28].

For the purpose of estimating the mean heritability (see Table 1, Figure 1 and S1 Table), we allowed the heritability estimates to take negative values (unconstrained model). Despite the lack of obvious biological interpretation of a negative heritability, it is an accepted procedure used in order to avoid bias in the estimated mean [10, 29]. Heritabilities are plotted as point estimates with bars that extend 2 times the estimated standard error up and down. Genes were considered to have heritability significantly different from 0 if the P value from GCTA was less than 0.05.

For comparing to BSLMM PVE, we restricted the GCTA heritability estimates to be within the [0,1] interval (constrained model, see Figures 3, 4 and 6).

Determining polygenicity versus sparsity using the elastic net

We used the *glmnet* R package to fit an elastic net model where the tuning parameter is chosen via 10 fold cross validation to maximize prediction performance measured by Pearson's R^2 [51, 52].

The elastic net penalty is controlled by mixing parameter α, which spans LASSO ($\alpha = 1$, the default) [18] at one extreme and ridge regression ($\alpha = 0$) [19] at the other. The ridge penalty shrinks the coefficients of correlated SNPs towards each other, while the LASSO tends to pick one of the correlated SNPs and discard the others. Thus, an optimal prediction R^2 for $\alpha = 0$ means the gene expression trait is highly polygenic, while an optimal prediction R^2 for $\alpha = 1$ means the trait is highly sparse.

In the DGN cohort, we tested 21 values of the mixing parameter ($\alpha = 0, 0.05, 0.1, ..., 0.90, 0.95, 1$) for optimal prediction of gene expression of the 341 genes on chromosome 22. In order to compare prediction R^2 values across α values, we used common folds and seeds for each run. For the rest of the autosomes in DGN and for whole tissue, cross-tissue, and tissue-specific expression in the GTEx cohort, we tested $\alpha = 0.05, 0.5, 1$.

Quantifying sparsity with Bayesian Sparse Linear Mixed Models (BSLMM)

We used BSLMM [24] to model the effect of local genetic variation (common SNPs within 1 Mb of gene) on the genetic architecture of gene expression. The BSLMM is a linear model with a polygenic component (small effects) and a sparse component (large effects) enforced by sparsity inducing priors on the regression coefficients [24]. BSLMM assumes the genotypic effects come from a mixture of two normal distributions and thus is flexible to both polygenic and sparse genetic architectures [24]. We used the software GEMMA [53] to implement BSLMM for each gene with 100K sampling steps per gene. The BSLMM estimates the PVE (the proportion of variance in phenotype explained by the additive genetic model, analogous to the heritability estimated in GCTA) and PGE (the proportion of genetic variance explained by the sparse effects terms where 0 means that genetic effect is purely polygenic and 1 means that the effect is purely sparse). From the second half of the sampling iterations for each gene, we report the median and the 95% credible sets of the PVE, PGE, and the $|\gamma|$ parameter (the number of SNPs with non-zero coefficients).

Orthogonal Tissue Decomposition (OTD)

We use a mixed effects model to decompose the expression level of a gene into a subject specific and subject by tissue-specific components. The expression of a gene g for individual i in tissue t, $Y_{i,t}$, is modeled as

$$Y_{i,t,g} = Y_{i,t} = Y_i^{\mathrm{CT}} + Y_{i,t}^{\mathrm{TS}} + \mathbf{Z}_i\boldsymbol{\beta} + \epsilon_{i,t}$$

where Y_i^{CT} is the random subject level intercept, $Y_{i,t}^{\mathrm{TS}}$ is the random subject by tissue intercept, $\mathbf{Z}_i$ represents covariates (for overall intercept, tissue intercept, gender, and PEER factors), and $\epsilon_{i,t}$ is the error term. We assume $Y_i^{\mathrm{CT}} \sim N(0, \sigma^2_{\mathrm{CT}})$, $Y_{i,t}^{\mathrm{TS}} \sim N(0, \sigma^2_{\mathrm{TS}})$, $\epsilon \sim N(0, \sigma^2_{\epsilon})$, and all three independent of each other. We fit the model one gene at a time and to simplify notation we keep the index g to be implicit and drop it from the equations.

For the cross-tissue component to be identifiable, multiple replicates of expression

are needed for each subject. In the same vein, for the tissue-specific component to be identifiable multiple replicates of expression is needed for a given tissue/subject pair. GTEx [27] data consisted of measurement of expression for multiple tissues for each subject, thus multiple replications per subject. However, there were very few replicated measurement for a given tissue/subject pair. Thus, we fit the reduced model and use the estimates of the residual as the tissue-specific component.

$$Y_{i,t} = Y_i^{\mathrm{CT}} + \mathbf{Z}_i\boldsymbol{\beta} + \epsilon_{i,t}$$

We consider the expression level of a gene at a given tissue for individual i to be composed of a cross tissue component which we represent as Y_i^{CT} and a tissue specific component, which given the lack of replications we estimate as the difference between the expression level and the cross tissue components (after adjusting for covariates).

The mixed effects model parameters were estimated using the `lme4` package [54] in R [55]. Batch effects and unmeasured confounders were accounted for using 15 `PEER` factors computed with the `PEER` [34] package in R. Posterior modes of the subject level random intercepts were used as estimates of the cross-tissue components whereas the residuals of the models were used as tissue-specific components.

The model included whole tissue gene expression levels in 8555 GTEx tissue samples from 544 unique subjects. A total of 17,647 Protein-coding genes (defined by GENCODE [50] version 18) with a mean gene expression level across tissues greater than 0.1 RPKM (reads per kilobase of transcript per million reads mapped) and RPKM > 0 in at least 3 individuals were included in the model.

OTD simulation

To test the robustness of our method, we derived simulated expression levels from the observed OTD components. The simulated expression phenotype is the sum of the observed OTD cross-tissue and tissue-specific components plus an error term derived by randomly sampling a normal distribution with standard deviation equal to the variance of each gene. [[Haky, put previous sentence in equation form after checking the above equations?]] We performed OTD on this simulated phenotype and compared the OTD-estimated cross-tissue and tissue-specific expression levels for each gene to the

true levels using Pearson correlation.

Comparison of OTD trait heritability with multi-tissue eQTL results

To verify that the newly derived cross-tissue and tissue-specific traits were capturing the expected properties, we used the results of the multi-tissue eQTL analysis performed by Flutre et al. [33] on nine tissues from the pilot phase of the GTEx project [27]. In particular, we used the posterior probability of a gene being actively regulated (PPA) in a tissue downloaded from the GTEx portal at `http://www.gtexportal.org/static/datasets/gtex_analysis_pilot_v3/multi_tissue_eqtls/Multi_tissue_eQTL_GTEx_Pilot_Phase_datasets.tar`. PPA can be interpreted as the probability a SNP is an eQTL in tissue t given the data. PPA is computed from a joint analysis of all tissues and takes account of sharing of eQTLs among tissues [33]. For example, consider a SNP showing modest association with expression in tissue t. If this SNP also shows strong association in the other tissues, then it will be assigned a higher probability of being an active eQTL in tissue t than if it showed no association in the other tissues [33].

We reasoned that genes with large cross-tissue component (i.e. high cross-tissue h^2) would have more uniform PPA across tissues. Thus we defined for each gene a measure of uniformity, U_g, across tissues based on the nine dimensional vector of PPAs using the entropy formula. More specifically, we divided each vector of PPA by their sum across tissues and computed the measure of uniformity as follows:

$$U_g = -\sum_t p_{t,g} \log p_{t,g}$$

where $p_{t,g}$ is the normalized PPA for gene g and tissue t.

Acknowledgments

We thank Nicholas Knoblauch and Jason Torres for initial pipeline development and planning. We thank Nicholas Miller for assistance building the results database.

GTEx data. The Genotype-Tissue Expression (GTEx) Project was supported by the Common Fund of the Office of the Director of the National Institutes of Health (commonfund.nih.gov/GTEx). Additional funds were provided by the NCI, NHGRI, NHLBI, NIDA, NIMH, and NINDS. Donors were enrolled at Biospecimen Source Sites funded by NCI Leidos Biomedical Research, Inc. subcontracts to the National Disease Research Interchange (10XS170), Roswell Park Cancer Institute (10XS171), and Science Care, Inc. (X10S172). The Laboratory, Data Analysis, and Coordinating Center (LDACC) was funded through a contract (HHSN268201000029C) to the The Broad Institute, Inc. Biorepository operations were funded through a Leidos Biomedical Research, Inc. subcontract to Van Andel Research Institute (10ST1035). Additional data repository and project management were provided by Leidos Biomedical Research, Inc.(HHSN261200800001E). The Brain Bank was supported supplements to University of Miami grant DA006227. Statistical Methods development grants were made to the University of Geneva (MH090941 & MH101814), the University of Chicago (MH090951,MH090937, MH101825, & MH101820), the University of North Carolina - Chapel Hill (MH090936), North Carolina State University (MH101819),Harvard University (MH090948), Stanford University (MH101782), Washington University (MH101810), and to the University of Pennsylvania (MH101822). The datasets used for the analyses described in this manuscript were obtained from dbGaP at `http://www.ncbi.nlm.nih.gov/gap` through dbGaP accession number phs000424.v3.p1.

DGN data. NIMH Study 88 – Data was provided by Dr. Douglas F. Levinson. We gratefully acknowledge the resources were supported by National Institutes of Health/National Institute of Mental Health grants 5RC2MH089916 (PI: Douglas F. Levinson, M.D.; Coinvestigators: Myrna M. Weissman, Ph.D., James B. Potash, M.D., MPH, Daphne Koller, Ph.D., and Alexander E. Urban, Ph.D.) and 3R01MH090941 (Co-investigator: Daphne Koller, Ph.D.).

Framingham data. The Framingham Heart Study is conducted and supported by the National Heart, Lung, and Blood Institute (NHLBI) in collaboration with Boston University (Contract No. N01-HC-25195 and HHSN268201500001I). This manuscript

was not prepared in collaboration with investigators of the Framingham Heart Study and does not necessarily reflect the opinions or views of the Framingham Heart Study, Boston University, or NHLBI.

Funding for SHARe Affymetrix genotyping was provided by NHLBI Contract N02-HL- 64278. SHARe Illumina genotyping was provided under an agreement between Illumina and Boston University. Funding for Affymetrix genotyping of the FHS Omni cohorts was provided by Intramural NHLBI funds from Andrew D. Johnson and Christopher J. O'Donnell.

Additional funding for SABRe was provided by Division of Intramural Research, NHLBI, and Center for Population Studies, NHLBI.

The following datasets were downloaded from dbGaP: phs000363.v12.p9 and phs000342.v13.p9.

Computing resources.

OSDC This work made use of the Open Science Data Cloud (OSDC) which is an Open Cloud Consortium (OCC)-sponsored project. This work was supported in part by grants from Gordon and Betty Moore Foundation and the National Science Foundation and major contributions from OCC members like the University of Chicago [56].

Bionimbus This work made use of the Bionimbus Protected Data Cloud (PDC), which is a collaboration between the Open Science Data Cloud (OSDC) and the IGSB (IGSB), the Center for Research Informatics (CRI), the Institute for Translational Medicine (ITM), and the University of Chicago Comprehensive Cancer Center (UCCCC). The Bionimbus PDC is part of the OSDC ecosystem and is funded as a pilot project by the NIH [57]
(`https://www.bionimbus-pdc.opensciencedatacloud.org/`).

References

1. Nicolae DL, Gamazon E, Zhang W, Duan S, Dolan ME, Cox NJ.
Trait-Associated SNPs Are More Likely to Be eQTLs: Annotation to Enhance

Discovery from GWAS. PLoS Genetics. 2010;6(4):e1000888. Available from: http://dx.doi.org/10.1371/journal.pgen.1000888.

2. Nica AC, Montgomery SB, Dimas AS, Stranger BE, Beazley C, Barroso I, et al. Candidate Causal Regulatory Effects by Integration of Expression QTLs with Complex Trait Genetic Associations. PLoS Genetics. 2010;6(4):e1000895. Available from: http://dx.doi.org/10.1371/journal.pgen.1000895.

3. Gusev A, Lee SH, Trynka G, Finucane H, Vilhjálmsson BJ, Xu H, et al. Partitioning Heritability of Regulatory and Cell-Type-Specific Variants across 11 Common Diseases. The American Journal of Human Genetics. 2014;95(5):535–552. Available from: http://dx.doi.org/10.1016/j.ajhg.2014.10.004.

4. Torres JM, Gamazon ER, Parra EJ, Below JE, Valladares-Salgado A, Wacher N, et al. Cross-tissue and tissue-specific eQTLs: partitioning the heritability of a complex trait. The American Journal of Human Genetics. 2014;95(5):521–534.

5. Davis LK, Yu D, Keenan CL, Gamazon ER, Konkashbaev AI, Derks EM, et al. Partitioning the heritability of Tourette syndrome and obsessive compulsive disorder reveals differences in genetic architecture. PLoS Genet. 2013;.

6. Albert FW, Kruglyak L. The role of regulatory variation in complex traits and disease. Nat Rev Genet. 2015;16(4):197–212. Available from: http://dx.doi.org/10.1038/nrg3891.

7. Stranger BE, Montgomery SB, Dimas AS, Parts L, Stegle O, Ingle CE, et al. Patterns of Cis Regulatory Variation in Diverse Human Populations. PLoS Genetics. 2012;8(4):e1002639. Available from: http://dx.doi.org/10.1371/journal.pgen.1002639.

8. Stranger BE, Nica AC, Forrest MS, Dimas A, Bird CP, Beazley C, et al. Population genomics of human gene expression. Nature Genetics. 2007;39(10):1217–1224. Available from: http://dx.doi.org/10.1038/ng2142.

9. Innocenti F, Cooper GM, Stanaway IB, Gamazon ER, Smith JD, Mirkov S, et al. Identification, Replication, and Functional Fine-Mapping of Expression

Quantitative Trait Loci in Primary Human Liver Tissue. PLoS Genetics. 2011;7(5):e1002078. Available from: http://dx.doi.org/10.1371/journal.pgen.1002078.

10. Wright FA, Sullivan PF, Brooks AI, Zou F, Sun W, Xia K, et al. Heritability and genomics of gene expression in peripheral blood. Nature Genetics. 2014 apr;46(5):430–437. Available from: http://dx.doi.org/10.1038/ng.2951.

11. Purcell SM, Wray NR, Stone JL, Visscher PM, O'Donovan MC, Sullivan PF, et al. Common polygenic variation contributes to risk of schizophrenia and bipolar disorder. Nature. 2009;Available from: http://dx.doi.org/10.1038/nature08185.

12. Stahl EA, Wegmann D, Trynka G, Gutierrez-Achury J, Do R, Voight BF, et al. Bayesian inference analyses of the polygenic architecture of rheumatoid arthritis. Nature Genetics. 2012;44(5):483–489. Available from: http://dx.doi.org/10.1038/ng.2232.

13. Morris AP, Voight BF, Teslovich TM, Ferreira T, Segrè AV, Steinthorsdottir V, et al. Large-scale association analysis provides insights into the genetic architecture and pathophysiology of type 2 diabetes. Nature Genetics. 2012;44(9):981–990. Available from: http://dx.doi.org/10.1038/ng.2383.

14. Gamazon ER, Wheeler HE, Shah KP, Mozaffari SV, Aquino-Michaels K, Carroll RJ, et al. A gene-based association method for mapping traits using reference transcriptome data. Nature Genetics. 2015;47(9):1091–1098. Available from: http://dx.doi.org/10.1038/ng.3367.

15. Brown CD, Mangravite LM, Engelhardt BE. Integrative modeling of eQTLs and cis-regulatory elements suggests mechanisms underlying cell type specificity of eQTLs. PLoS Genet. 2013;9(8):e1003649.

16. King EG, Sanderson BJ, McNeil CL, Long AD, Macdonald SJ. Genetic dissection of the Drosophila melanogaster female head transcriptome reveals widespread allelic heterogeneity. PLoS Genet. 2014;10(5):e1004322.

17. Zhang X, Cal AJ, Borevitz JO. Genetic architecture of regulatory variation in Arabidopsis thaliana. Genome research. 2011;21(5):725–733.

18. Tibshirani R. Regression Shrinkage and Selection via the Lasso. Journal of the Royal Statistical Society Series B (Methodological). 2015;58(1):267–288. Available from: http://www.jstor.org/stable/2346178.

19. Hoerl AE, Kennard RW. Ridge Regression: Applications to Nonorthogonal Problems. Technometrics. 1970;12(1):69–82. Available from: http://dx.doi.org/10.1080/00401706.1970.10488635.

20. de los Campos G, Gianola D, Allison DB. Predicting genetic predisposition in humans: the promise of whole-genome markers. Nat Rev Genet. 2010;11(12):880–886. Available from: http://dx.doi.org/10.1038/nrg2898.

21. Wheeler HE, Aquino-Michaels K, Gamazon ER, Trubetskoy VV, Dolan ME, Huang RS, et al. Poly-Omic Prediction of Complex Traits: OmicKriging. Genetic Epidemiology. 2014;38(5):402–415. Available from: http://dx.doi.org/10.1002/gepi.21808.

22. Zou H, Hastie T. Regularization and variable selection via the elastic net. Journal of the Royal Statistical Society: Series B (Statistical Methodology). 2005;67(2):301–320. Available from: http://dx.doi.org/10.1111/j.1467-9868.2005.00503.x.

23. Abraham G, Kowalczyk A, Zobel J, Inouye M. Performance and robustness of penalized and unpenalized methods for genetic prediction of complex human disease. Genetic Epidemiology. 2013;37(2):184–195.

24. Zhou X, Carbonetto P, Stephens M. Polygenic Modeling with Bayesian Sparse Linear Mixed Models. PLoS Genetics. 2013;9(2):e1003264. Available from: http://dx.doi.org/10.1371/journal.pgen.1003264.

25. Cheung VG, Spielman RS, Ewens KG, Weber TM, Morley M, Burdick JT. Mapping determinants of human gene expression by regional and genome-wide association. Nature. 2005;437(7063):1365–1369. Available from: http://dx.doi.org/10.1038/nature04244.

26. Battle A, Mostafavi S, Zhu X, Potash JB, Weissman MM, McCormick C, et al. Characterizing the genetic basis of transcriptome diversity through RNA-sequencing of 922 individuals. Genome Research. 2013;24(1):14–24. Available from: http://dx.doi.org/10.1101/gr.155192.113.

27. Ardlie KG, Deluca DS, Segre AV, Sullivan TJ, Young TR, Gelfand ET, et al. The Genotype-Tissue Expression (GTEx) pilot analysis: Multitissue gene regulation in humans. Science. 2015;348(6235):648–660. Available from: http://dx.doi.org/10.1126/science.1262110.

28. Yang J, Lee SH, Goddard ME, Visscher PM. GCTA: A Tool for Genome-wide Complex Trait Analysis. The American Journal of Human Genetics. 2011;88(1):76–82. Available from: http://dx.doi.org/10.1016/j.ajhg.2010.11.011.

29. Price AL, Helgason A, Thorleifsson G, McCarroll SA, Kong A, Stefansson K. Single-Tissue and Cross-Tissue Heritability of Gene Expression Via Identity-by-Descent in Related or Unrelated Individuals. PLoS Genetics. 2011;7(2):e1001317. Available from: http://dx.doi.org/10.1371/journal.pgen.1001317.

30. Pierce BL, Tong L, Chen LS, Rahaman R, Argos M, Jasmine F, et al. Mediation Analysis Demonstrates That Trans-eQTLs Are Often Explained by Cis-Mediation: A Genome-Wide Analysis among 1,800 South Asians. PLoS genetics. 2014;10(12):e1004818.

31. Zhang X, Joehanes R, Chen BH, Huan T, Ying S, Munson PJ, et al. Identification of common genetic variants controlling transcript isoform variation in human whole blood. Nature Genetics. 2015;47(4):345–352. Available from: http://dx.doi.org/10.1038/ng.3220.

32. Speed D, Hemani G, Johnson MR, Balding DJ. Improved heritability estimation from genome-wide SNPs. The American Journal of Human Genetics. 2012;91(6):1011–1021.

33. Flutre T, Wen X, Pritchard J, Stephens M. A Statistical Framework for Joint eQTL Analysis in Multiple Tissues. PLoS Genetics. 2013;9(5):e1003486. Available from: http://dx.doi.org/10.1371/journal.pgen.1003486.

34. Stegle O, Parts L, Piipari M, Winn J, Durbin R. Using probabilistic estimation of expression residuals (PEER) to obtain increased power and interpretability of gene expression analyses. Nat Protoc. 2012;7(3):500–507. Available from: http://dx.doi.org/10.1038/nprot.2011.457.

35. Leek JT, Storey JD. Capturing heterogeneity in gene expression studies by surrogate variable analysis. PLoS Genet. 2007;3(9):1724–1735.

36. Manor O, Segal E. Robust prediction of expression differences among human individuals using only genotype information. PLoS Genet. 2013;9(3):e1003396.

37. Gusev A, Ko A, Shi H, Bhatia G, Chung W, Penninx BW, et al. Integrative approaches for large-scale transcriptome-wide association studies. Nature genetics. 2016;.

38. Zhu Z, Zhang F, Hu H, Bakshi A, Robinson MR, Powell JE, et al. Integration of summary data from GWAS and eQTL studies predicts complex trait gene targets. Nature genetics. 2016;.

39. Giambartolomei C, Vukcevic D, Schadt EE, Franke L, Hingorani AD, Wallace C, et al. Bayesian test for colocalisation between pairs of genetic association studies using summary statistics. PLoS Genet. 2014;10(5):e1004383.

40. He X, Fuller CK, Song Y, Meng Q, Zhang B, Yang X, et al. Sherlock: detecting gene-disease associations by matching patterns of expression QTL and GWAS. The American Journal of Human Genetics. 2013;92(5):667–680.

41. Howie B, Fuchsberger C, Stephens M, Marchini J, Abecasis GR. Fast and accurate genotype imputation in genome-wide association studies through pre-phasing. Nature Genetics. 2012;44(8):955–959. Available from: http://dx.doi.org/10.1038/ng.2354.

42. Fuchsberger C, Abecasis GR, Hinds DA. minimac2: faster genotype imputation. Bioinformatics. 2014;31(5):782–784. Available from: http://dx.doi.org/10.1093/bioinformatics/btu704.

43. Irizarry RA, Bolstad BM, Collin F, Cope LM, Hobbs B, Speed TP. Summaries of Affymetrix GeneChip probe level data. Nucleic acids research. 2003;31(4):e15–e15.

44. MacDonald JW. huex10stprobeset.db: Affymetrix huex10 annotation data (chip huex10stprobeset). R package;version 8.3.1.

45. MacDonald JW. huex10sttranscriptcluster.db: Affymetrix huex10 annotation data (chip huex10sttranscriptcluster). R package;version 8.3.1.

46. Chang CC, Chow CC, Tellier L, Vattikuti S, Purcell SM, Lee JJ. Second-generation PLINK: rising to the challenge of larger and richer datasets. Gigascience. 2015;4(7).

47. Delaneau O, Marchini J, Zagury JF. A linear complexity phasing method for thousands of genomes. Nature methods. 2012;9(2):179–181.

48. McCarthy S, Das S, Kretzschmar W, Durbin R, Abecasis G, Marchini J. A reference panel of 64,976 haplotypes for genotype imputation. bioRxiv. 2015;p. 035170.

49. Shabalin AA. Matrix eQTL: ultra fast eQTL analysis via large matrix operations. Bioinformatics. 2012;28(10):1353–1358.

50. Harrow J, Frankish A, Gonzalez JM, Tapanari E, Diekhans M, Kokocinski F, et al. GENCODE: The reference human genome annotation for The ENCODE Project. Genome Research. 2012;22(9):1760–1774. Available from: http://dx.doi.org/10.1101/gr.135350.111.

51. Friedman J, Hastie T, Tibshirani R. Regularization Paths for Generalized Linear Models via Coordinate Descent. Journal of Statistical Software. 2010;33(1):1–22. Available from: http://www.jstatsoft.org/v33/i01/.

52. Simon N, Friedman J, Hastie T, Tibshirani R. Regularization Paths for Cox's Proportional Hazards Model via Coordinate Descent. Journal of Statistical

Software. 2011;39(5):1–13. Available from: http://www.jstatsoft.org/v39/i05/.

53. Zhou X, Stephens M. Genome-wide efficient mixed-model analysis for association studies. Nature Genetics. 2012;44(7):821–824. Available from: http://dx.doi.org/10.1038/ng.2310.

54. Bates D, Mächler M, Bolker BM, Walker S. Fitting Linear Mixed-Effects Models using lme4. Journal of Statistical Software. 2015;67(1):1–48. Available from: http://dx.doi.org/10.18637/jss.v067.i01.

55. R Core Team. R: A Language and Environment for Statistical Computing. Vienna, Austria; 2015. Available from: http://www.R-project.org/.

56. Grossman RL, Greenway M, Heath AP, Powell R, Suarez RD, Wells W, et al. The design of a community science cloud: The open science data cloud perspective. In: High Performance Computing, Networking, Storage and Analysis (SCC), 2012 SC Companion:. IEEE; 2012. p. 1051–1057.

57. Heath AP, Greenway M, Powell R, Spring J, Suarez R, Hanley D, et al. Bionimbus: a cloud for managing, analyzing and sharing large genomics datasets. Journal of the American Medical Informatics Association. 2014;21(6):969–975.

Supporting Information

S1 Fig

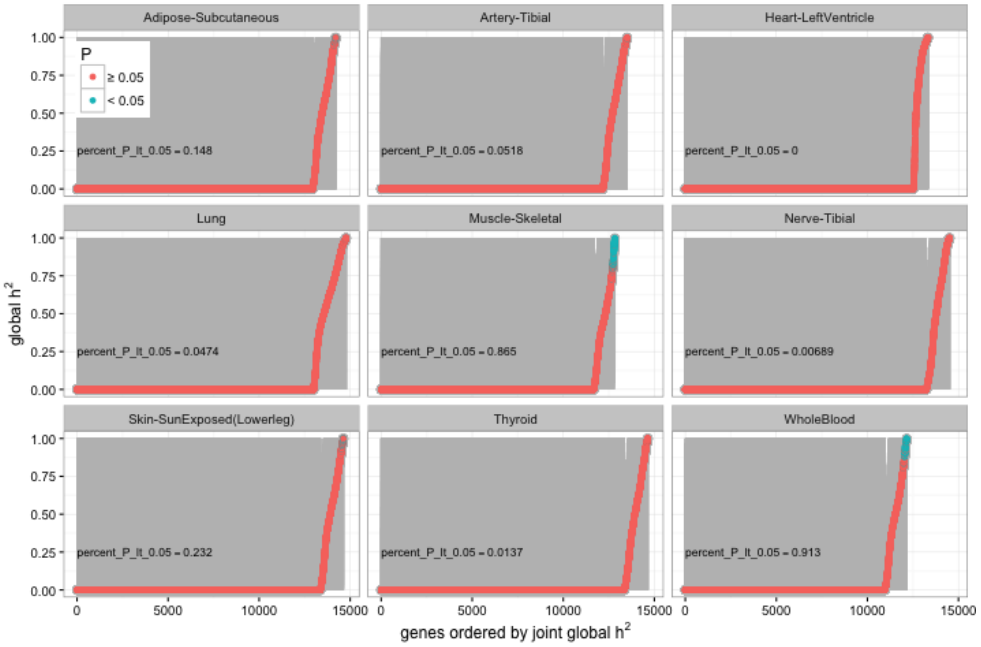

GTEx whole tissue distal heritability (h^2) estimation. Distal (SNPs that are eQTLs in the Framingham Heart Study on other chromosomes [FDR < 0.05]) gene expression h^2 estimates from a joint model in the nine GTEx tissues with the largest sample sizes are ordered by increasing h^2. The 95% confidence interval (CI) of each h^2 estimate is in gray and significant genes ($P < 0.05$) are in blue. Less than 1% of genes show significant distal h^2.

S2 Fig

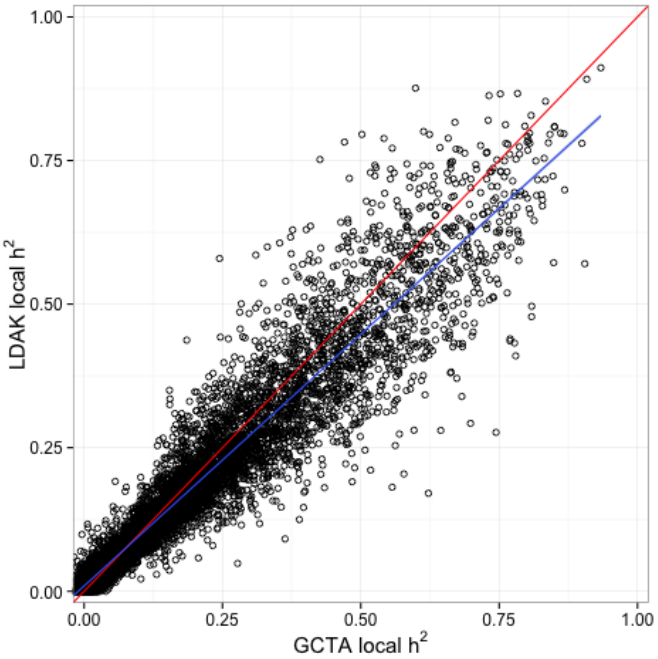

DGN local heritability estimation comparison between LDAK and GCTA. The Pearson correlation between GCTA and the LD-adjusted kinship local h^2 estimates of gene expression is 0.96. In red is the identity line and in blue is the best fit linear regression line, which indicates that on average, the GCTA estimates are slightly higher than the LDAK estimates.

S3 Fig

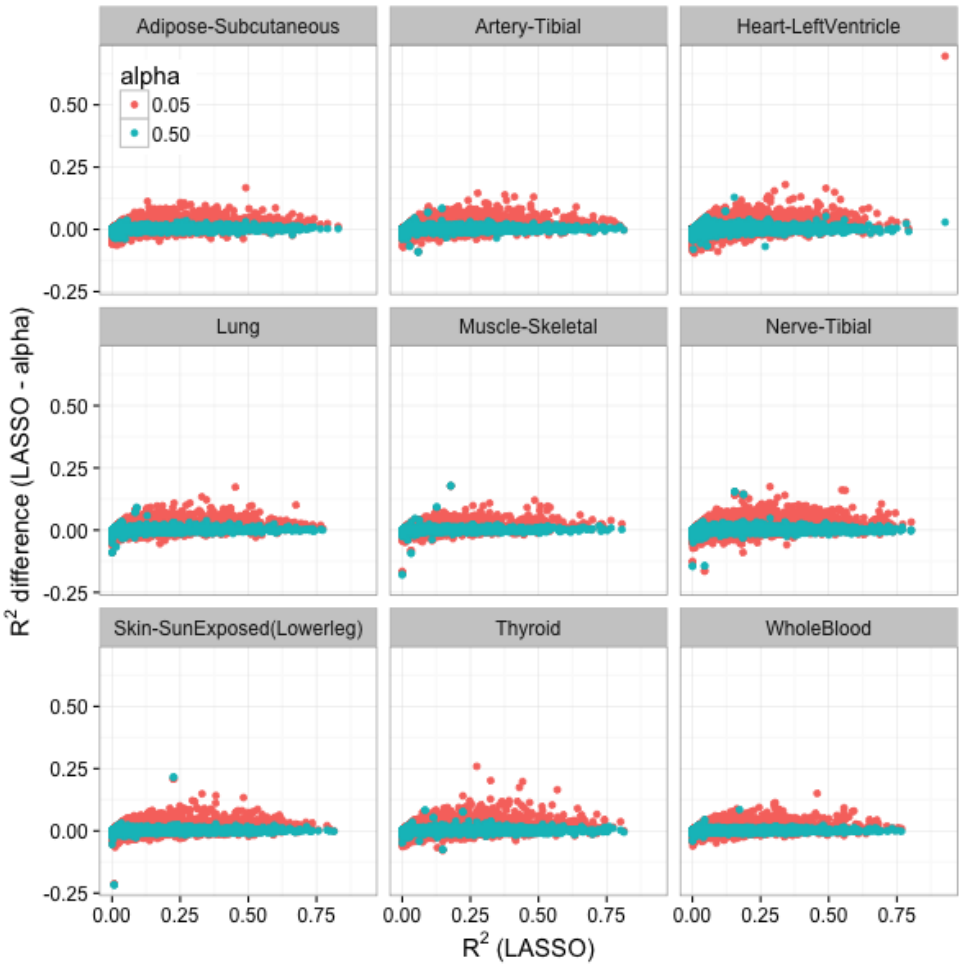

GTEx whole tissue cross-validated predictive performance across the elastic net. The difference between the cross validated R^2 of the LASSO model and the elastic net model mixing parameters 0.05 and 0.5 for autosomal protein coding genes per tissue. Elastic net with $\alpha = 0.5$ values hover around zero, meaning that it has similar predictive performance to LASSO. The R^2 difference of the more polygenic model (elastic net with $\alpha = 0.05$) is mostly above the 0 line, indicating that this model performs worse than the LASSO model across tissues.

S4 Fig

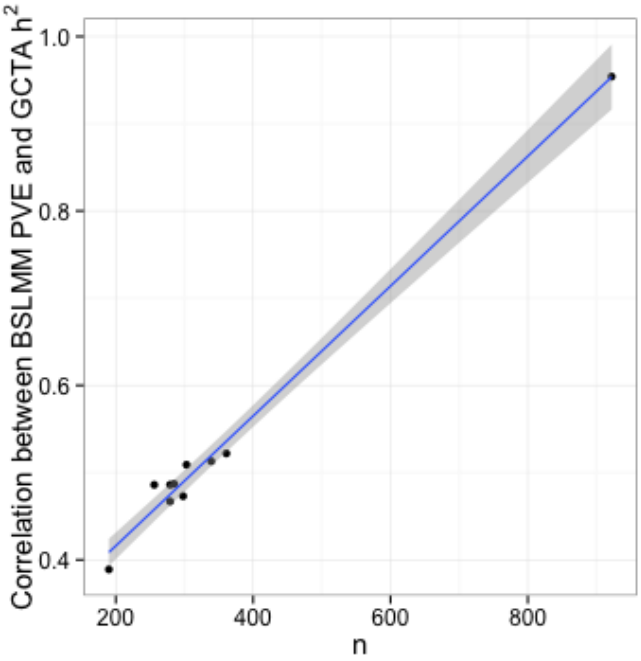

Correlation between heritability models compared to sample size. The Pearson correlation between estimates of heritability using BSLMM vs. GCTA is dependent on sample size (R = 0.99, $P = 3x10^{-9}$).

S5 Fig

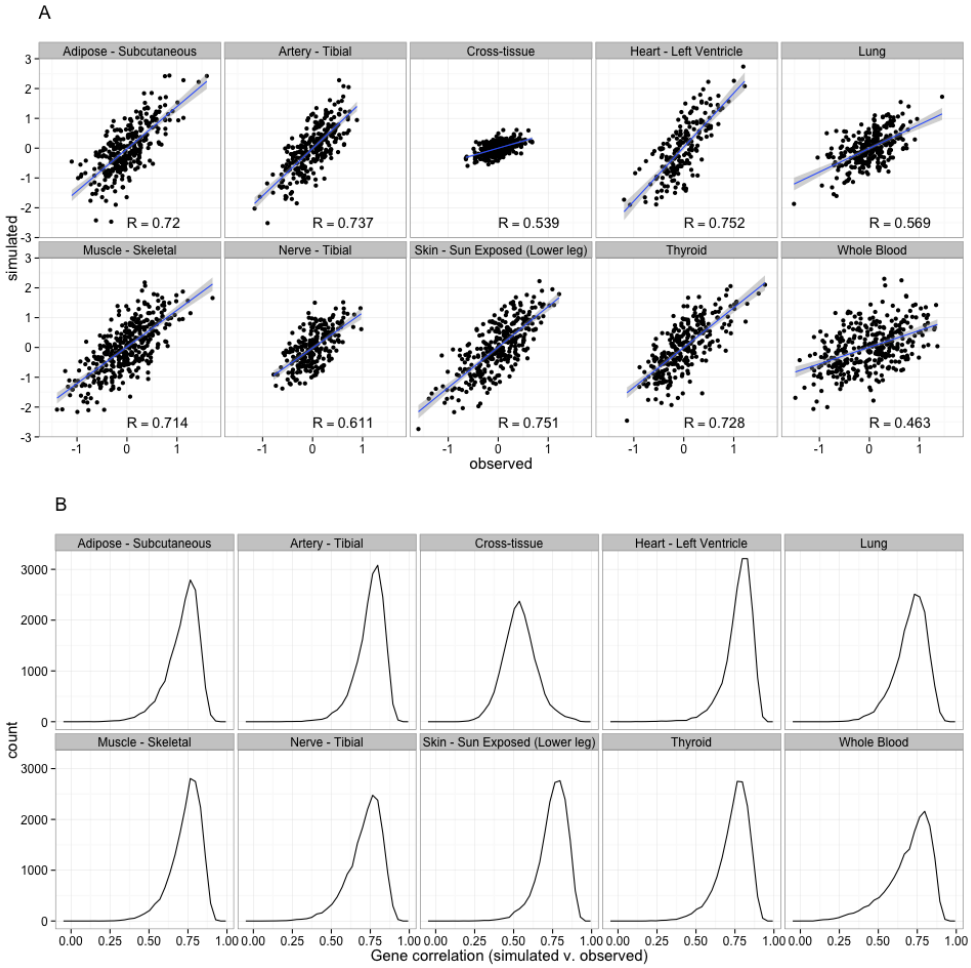

Identifiability of cross tissue and tissue specific components shown in simulated data. The simulated phenotype is the sum of the observed cross-tissue and tissue-specific components (estimated via OTD in the observed data) plus an error term derived by randomly sampling a normal distribution with variance equal to the variance of each gene. **(A)** Correlation between true and OTD-estimated cross tissue and tissue specific components for one gene, *SLTM*. **(B)** Histogram of the correlation between true and OTD-estimated components across all genes.

S6 Fig

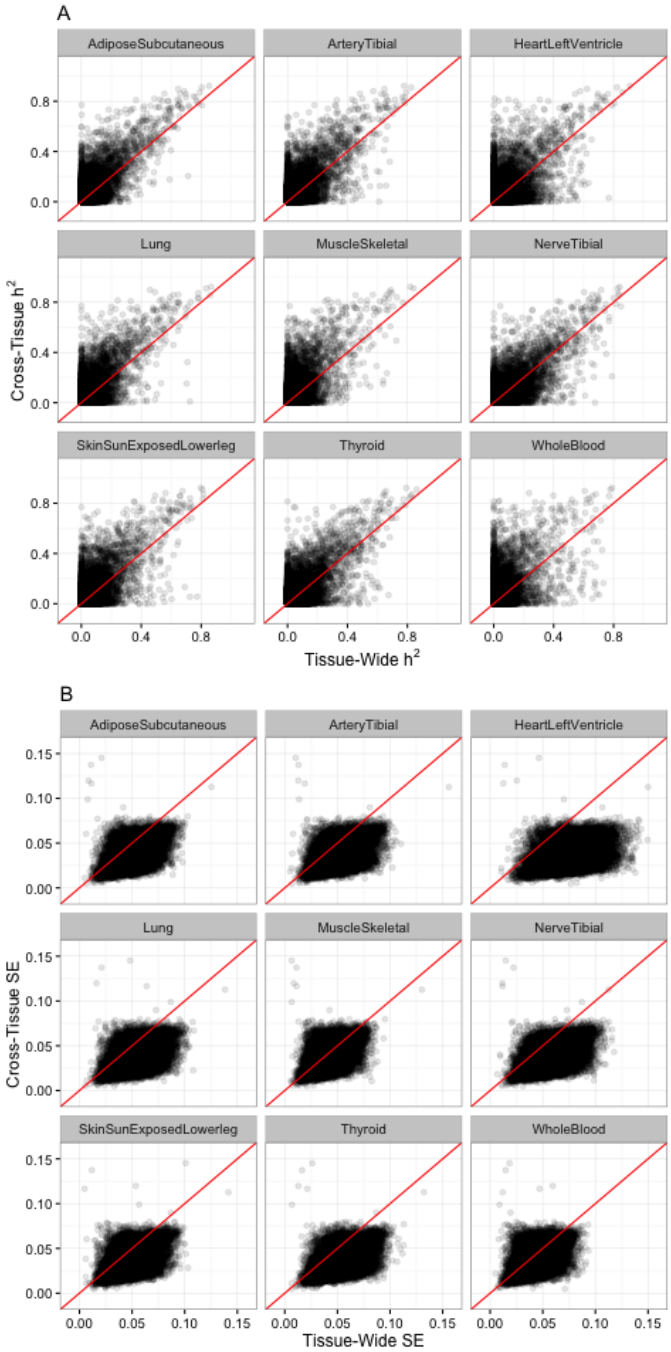

Cross-tissue and whole tissue comparison of heritability (h^2, A) and standard error (SE, B). Cross-tissue local h^2 is estimated using the cross-tissue component (random effects) of the mixed effects model for gene expression and SNPs within 1 Mb of each gene. Whole tissue local h^2 is estimated using the measured gene expression for each respective tissue and SNPs within 1 Mb of each gene. Estimates of h^2 for cross-tissue expression traits are larger and their standard errors are smaller than the corresponding estimates for each whole tissue expression trait.

S7 Fig

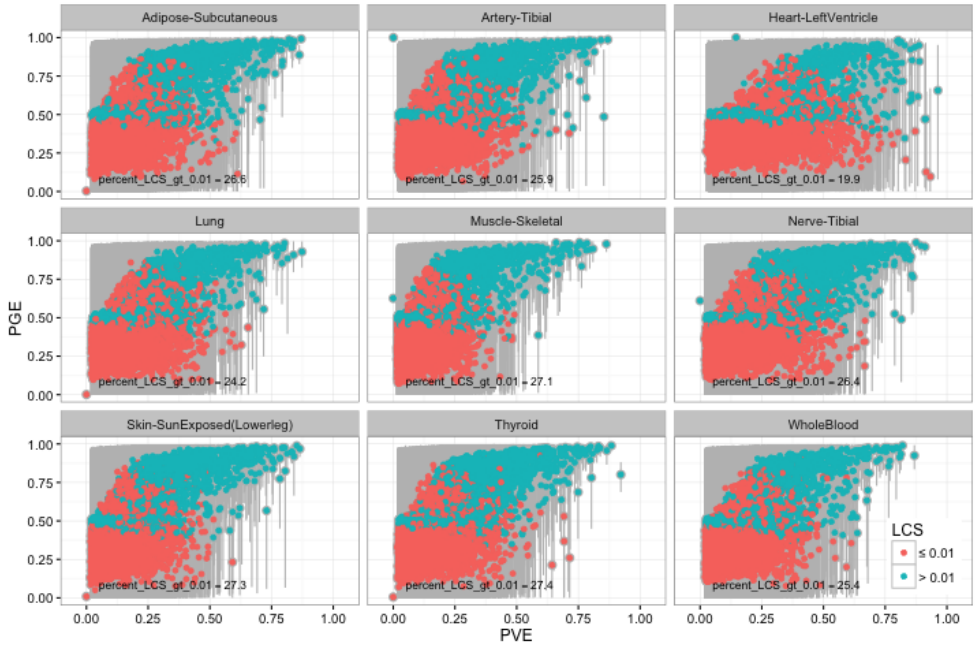

GTEx whole tissue expression Bayesian Sparse Linear Mixed Model. Comparison of median PGE (proportion of PVE explained by sparse effects) to median PVE (total proportion of variance explained, the BSLMM equivalent of h^2) for expression of each gene. The 95% credible set of each PGE estimate is in gray and genes with a lower credible set (LCS) greater than 0.01 are in blue. For highly heritable genes the sparse component is close to 1, thus for high heritability genes the local architecture is sparse across tissues. For lower heritability genes, there is not enough evidence to determine sparsity or polygenicity.

S8 Fig

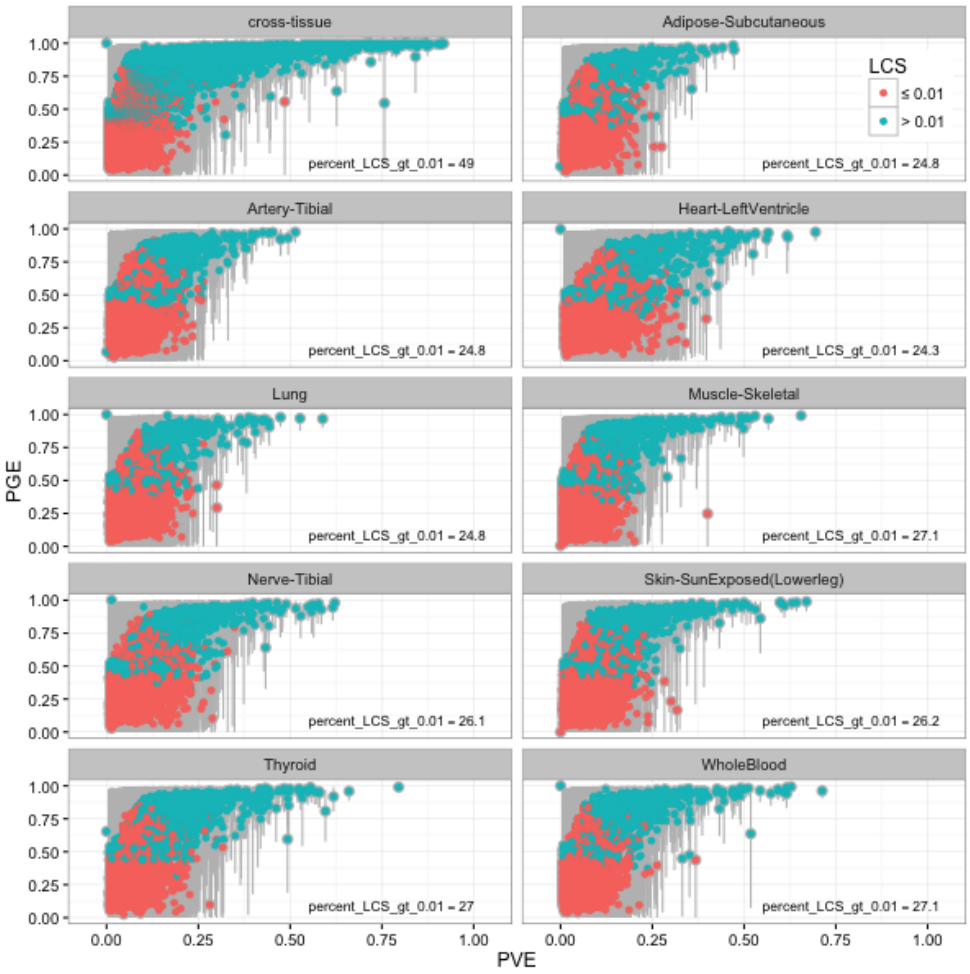

GTEx orthogonal tissue decomposition cross-tissue and tissue-specific expression Bayesian Sparse Linear Mixed Model. Comparison of median PGE (proportion of PVE explained by sparse effects) to median PVE (total proportion of variance explained, the BSLMM equivalent of h^2) for expression of each gene. The 95% credible set of each PGE estimate is in gray and genes with a lower credible set (LCS) greater than 0.01 are in blue. For highly heritable genes the sparse component is close to 1, thus for high heritability genes the local architecture is sparse across tissues. About twice as many cross-tissue expression traits have significant PGE (LCS > 0.01) compared to the tissue-specific expression traits.

S9 Fig

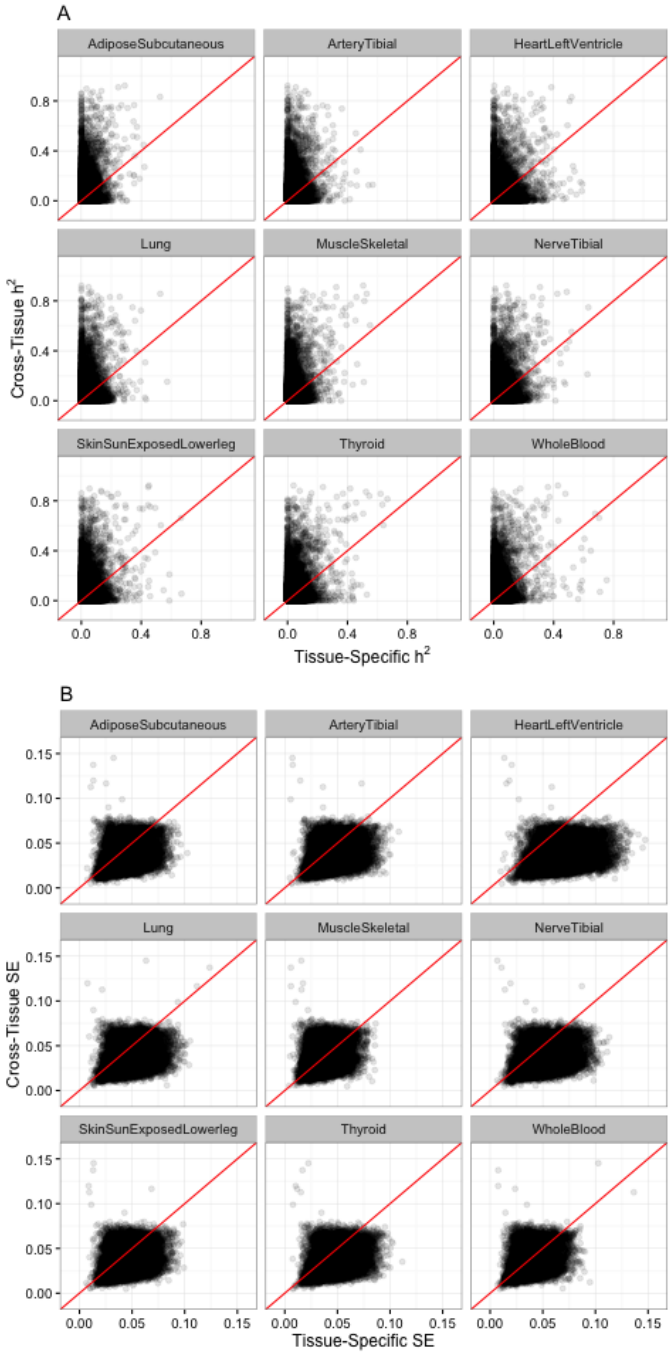

Cross-tissue and tissue-specific comparison of heritability (h^2, A) and standard error (SE, B) estimation. Cross-tissue local h^2 is estimated using the cross-tissue component (random effects) of the mixed effects model for gene expression and SNPs within 1 Mb of each gene. Tissue-specifc local h^2 is estimated using the tissue-specific component (residuals) of the mixed effects model for gene expression for each respective tissue and SNPs within 1 Mb of each gene. Estimates of h^2 for cross-tissue expression traits are larger and their standard errors are smaller than the corresponding estimates for each tissue-specific expression trait.

S10 Fig

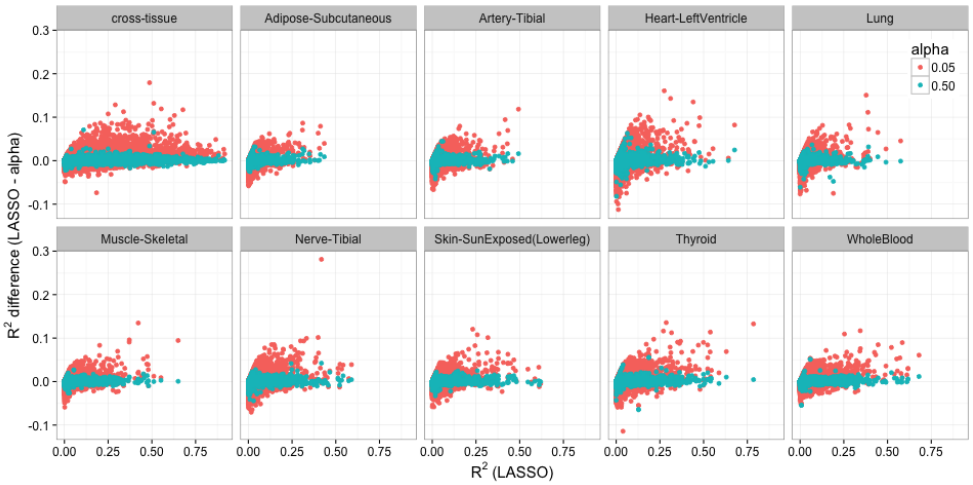

GTEx orthogonal tissue decomposition cross-tissue and tissue-specific expression cross-validated predictive performance across the elastic net. The difference between the cross validated R^2 of the LASSO model and the elastic net model mixing parameters 0.05 and 0.5 for autosomal protein coding genes per cross-tissue and tissue-specific gene expression traits. Elastic net with $\alpha = 0.5$ values hover around zero, meaning that it has similar predictive performance to LASSO. The R^2 difference of the more polygenic model (elastic net with $\alpha = 0.05$) is mostly above the 0 line, indicating that this model performs worse than the LASSO model across decomposed tissues.

S11 Fig

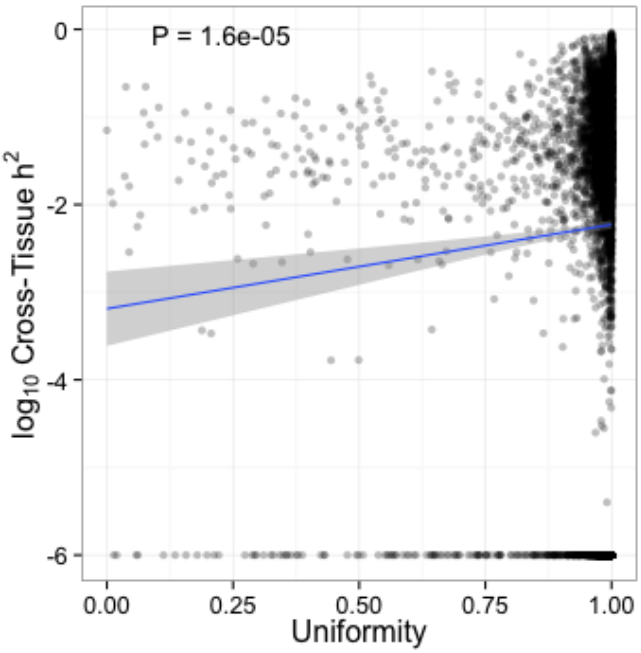

Continuous distribution of heritability of the cross-tissue component vs. a measure of uniformity of genetic regulation across tissues. The measure of uniformity was computed using the posterior probability of a gene being actively regulated in a tissue, PPA, from the Flutre et al. [33] multi-tissue eQTL analysis. Genes with PPA concentrated in one tissue were assigned small values of the uniformity measure whereas genes with PPA uniformly distributed across tissues were assigned high value of uniformity measure. See Methods for the entropy-based definition of uniformity. The blue line is the best fit linear regression and shows a significant positive correlation between h^2 and uniformity ($\beta = 0.96$, $P = 1.6e-05$).

S1 Table

S1 Table. Estimates of cross-tissue and tissue-specific local h^2. Expression levels derived by Orthogonal Tissue Decomposition and h^2 estimated using the `--reml-no-constrain` method.

tissue	n	mean h^2 (SE)	% $P < 0.05$	num $P < 0.05$	num expressed
Cross-tissue	450	0.062 (0.0008)	35.4	6003	16951
Adipose - Subcutaneous	298	0.017 (0.0004)	10.3	1747	16951
Adrenal Gland	126	0.037 (0.0007)	10.2	1731	16951
Artery - Aorta	198	0.022 (0.0005)	10.2	1733	16951
Artery - Coronary	119	0.048 (0.0008)	12.2	2066	16951
Artery - Tibial	285	0.022 (0.0004)	13.3	2262	16951
Brain - Anterior cingulate cortex (BA24)	72	0.037 (0.0012)	8.6	1451	16951
Brain - Caudate (basal ganglia)	100	0.042 (0.0009)	9.8	1659	16951
Brain - Cerebellar Hemisphere	89	0.046 (0.0011)	10.2	1730	16951
Brain - Cerebellum	103	0.041 (0.0009)	10.8	1825	16951
Brain - Cortex	96	0.053 (0.0010)	10.6	1803	16951
Brain - Frontal Cortex (BA9)	92	0.037 (0.0009)	8.4	1418	16951
Brain - Hippocampus	81	0.033 (0.0010)	7.6	1292	16951
Brain - Hypothalamus	81	0.020 (0.0011)	7.8	1321	16951
Brain - Nucleus accumbens (basal ganglia)	93	0.040 (0.0010)	8.9	1511	16951
Brain - Putamen (basal ganglia)	82	0.033 (0.0010)	7.8	1323	16951
Breast - Mammary Tissue	183	0.020 (0.0005)	7.7	1307	16951
Cells - EBV-transformed lymphocytes	115	0.045 (0.0008)	10.8	1833	16951
Cells - Transformed fibroblasts	272	0.019 (0.0004)	10.6	1805	16951
Colon - Sigmoid	124	0.024 (0.0007)	9.0	1530	16951
Colon - Transverse	170	0.022 (0.0005)	8.6	1462	16951
Esophagus - Gastroesophageal Junction	127	0.029 (0.0007)	8.9	1512	16951
Esophagus - Mucosa	242	0.026 (0.0005)	13.7	2319	16951
Esophagus - Muscularis	219	0.024 (0.0005)	11.0	1871	16951
Heart - Atrial Appendage	159	0.031 (0.0006)	9.4	1601	16951
Heart - Left Ventricle	190	0.025 (0.0005)	11.2	1894	16951
Liver	98	0.036 (0.0009)	8.9	1506	16951
Lung	279	0.018 (0.0004)	10.7	1819	16951
Muscle - Skeletal	361	0.020 (0.0003)	13.1	2223	16951
Nerve - Tibial	256	0.026 (0.0004)	13.3	2250	16951
Ovary	85	0.043 (0.0009)	7.8	1323	16951
Pancreas	150	0.036 (0.0007)	11.6	1969	16951
Pituitary	87	0.044 (0.0010)	9.4	1590	16951
Skin - Not Sun Exposed (Suprapubic)	196	0.041 (0.0005)	19.2	3249	16951
Skin - Sun Exposed (Lower leg)	303	0.027 (0.0004)	17.3	2939	16951
Small Intestine - Terminal Ileum	77	0.046 (0.0011)	7.9	1340	16951
Spleen	89	0.062 (0.0010)	10.7	1820	16951
Stomach	171	0.020 (0.0005)	8.3	1406	16951
Testis	157	0.042 (0.0007)	14.0	2378	16951
Thyroid	279	0.024 (0.0004)	13.3	2250	16951
Whole Blood	339	0.025 (0.0004)	17.7	3004	16951

All tissues are from the GTEx Project. Mean heritability (h^2) and the standard error of the mean (SE) are calculated across genes for each tissue. The percentage (%) and number (num) of genes with significant h^2 estimates ($P < 0.05$) and the number of genes expressed in each tissue are also reported.